Acta Pharmaceutica Sinica B 2025;15(4):2197−2216

Chinese Pharmaceutical Association
Institute of Materia Medica, Chinese Academy of Medical Sciences

Acta Pharmaceutica Sinica B

www.elsevier.com/locate/apsb
www.sciencedirect.com

ORIGINAL ARTICLE

Microneedle delivery platform integrated with *Staphylococcus epidermidis*-derived extracellular vesicles-based nanoantibiotics for efficient bacterial infection atopic dermatitis treatment

Hong Zhou[a], Shuting Zhang[a], Xinxin Liu[b], Aiping Feng[b], Siyuan Chen[c,*], Wei Liu[a,*]

[a]*National Engineering Research Center for Nanomedicine, College of Life Science and Technology, Huazhong University of Science and Technology, Wuhan 430074, China*
[b]*Department of Dermatology, Union Hospital, Tongji Medical College, Huazhong University of Science and Technology, Wuhan 430074, China*
[c]*Research Institute for Biomaterials, Tech Institute for Advanced Materials Bioinspired Biomedical Materials & Devices Center, College of Materials Science and Engineering, Jiangsu Collaborative Innovation Center for Advanced Inorganic Function Composites, Suqian Advanced Materials Industry Technology Innovation Center, Nanjing Tech University, Nanjing 211816, China*

Received 15 September 2024; received in revised form 20 December 2024; accepted 14 January 2025

KEY WORDS

Skin microbiota;
Staphylococcus epidermidis;
Extracellular vesicles;
Nanoantibiotics;
Microneedle;
Staphylococcus aureus;
Bacterial infection;
Atopic dermatitis

Abstract Due to the difficulty of overcoming the abnormal epidermal barriers and addressing *S. aureus* infections without disrupting indigenous skin microbiota, effective treatment of bacterial infection atopic dermatitis (AD) remains a significant clinical challenge. Skin microbiota-derived extracellular vesicles (EVs) shows protentional for skin disease treatment, but the lack of antimicrobial activity and limited skin penetration hamper their application in bacterial infection AD treatment. Here, we developed novel nanoantibiotics by loading Lev into *S. epidermidis*-derived EVs (Lev@SE-EVs), with supreme antimicrobial activity, regulating epidermal immune responses and enhanced epidermal barrier functionality. The nanoantibiotics were further integrated into hyaluronic acid-based microneedle (MN) for efficient transdermal delivery of therapeutic agents and effectively treating bacterial infection in AD. Upon insertion into the skin, the rapidly released Lev@SE-EVs from MN are uptake by *S. aureus* in a selective manner, fibroblasts, and surrounding immune cells to exert therapeutic effects in the infected dermal layer, resulting in mitigated skin inflammation, reduced *S. aureus* burden and increased dermis repair. Notably, Lev@SE-EVs induce IL-17A$^+$ CD8$^+$ T-cell

*Corresponding authors.
E-mail addresses: siyuan.chen@njtech.edu.cn (Siyuan Chen), wliu@hust.edu.cn (Wei Liu).

Peer review under the responsibility of Chinese Pharmaceutical Association and Institute of Materia Medica, Chinese Academy of Medical Sciences.

https://doi.org/10.1016/j.apsb.2025.02.038

accumulation in the skin in an unrelated inflammation manner, which may represent heterologous protection. This EVs-integrated MN assisted Lev@SE-EVs to alleviate skin inflammation, repair skin, and provide an effective and safe therapeutic approach for bacterial infection AD treatment.

1. Introduction

Atopic dermatitis (AD), a common chronic inflammatory skin disorder is characterized by relapsing, dryness, itchy, and inflamed skin, and is often infected by *S. aureus*, affecting 10%−30% of children in industrialized countries[1,2]. Among its various subtypes, bacterial infection-associated AD poses significant clinical challenges due to the abnormalities of the epidermal barrier and dermal dysbiosis by *S. aureus*[3,4]. Addressing bacterial infections is of crucial importance for the treatment of bacterial infection-associated AD. While antibiotic treatments, such as levofloxacin (Lev), are an important component of the management of this subtype in clinical practice, their efficacy is limited and may lead to an increased risk of secondary infections[5-7]. Anti-inflammatory or immunosuppressive drugs, while helpful in symptom relief, can mask signs of infection, delay diagnosis, and potentially worsen the infection by allowing it to spread[8]. Although combination therapies, including antibiotics along with anti-inflammatory or immunosuppressive agents, are commonly used[9,10], they often lead to increased risk of adverse reactions, drug interactions, the development of bacterial resistance, and more harm to the indigenous skin microbiota by nonspecific killing[11,12]. Besides, managing multiple medications simultaneously can lead to challenges in patient compliance and medication adherence, and the complexity of treatment regimens may also contribute to medication errors and dosing inaccuracies[3,13,14]. Therefore, a novel and simple therapy that could effectively treat bacterial infection AD and in the meantime maintain the stability of indigenous skin microbiota is urgently required.

S. epidermidis, a prevalent constituent of commensal skin bacteria on healthy human skin, is vital in protecting skin health. *S. epidermidis* can mitigate inflammation after skin injury, promote skin wound healing, stimulate antimicrobial peptide (AMP) expression by keratinocytes, and induce the development of cutaneous T cells[15-18]. In addition to constitutively expressed AMPs, some specific strains can produce their AMPs which could selectively kill *S. aureus*[19]. A recent study demonstrates a link between worsening AD and the loss of *S. epidermidis*[9]. Hence, the application of this bacterium for AD treatment represents a valid strategy for rational microbiome therapy[19-21]. For example, *S. epidermidis* can generate protective ceramides to promote skin barrier homeostasis in an uninfected AD mouse model[22]. Notably, the application of *S. epidermidis* strains with *S. aureus*-targeting AMP secretion functionality can decrease *S. aureus* on the skin surface in bacterial infection AD subjects, while the ones without this ability can not[19]. Although this approach bypasses the drawbacks of combination therapy, several limitations need to be addressed to apply *S. epidermidis* in the treatment of bacterial infection AD. Randomized screening of the strains with anti-*S. aureus* activity is costly. Furthermore, the application of the bacterium is unable to deal with dermal dysbiosis due to the skin barrier effect. Most importantly, there are potential safety issues for the application of live bacteria such as increased skin IgE levels and the signs of increased inflammation[22].

Extracellular vesicles (EVs) have emerged as desirable candidates for therapeutic intervention in dermatology[23,24]. Recently, skin microbiota-derived EVs have attracted growing interest. Due to carrying a variety of cargos (such as lipids, proteins, and nucleic acids) from parental cells, EVs show similar functionalities as the parental cells. Our previous research has shown that akin to *S. epidermidis*, *S. epidermidis*-derived EVs (SE-EVs) trigger inflammation when existing below the dermis but are tolerated on the epidermis, and induce AMPs secretion by keratinocytes and specific T-cell responses against invasive pathogens[25]. We also have demonstrated the vital roles of SE-EVs-mediated signaling biomolecules for alleviating inflammation in uninfected AD models, similar to other publications[25,26]. More importantly, we found that due to being non-replicative, SE-EVs mitigate cutaneous inflammation in uninfected AD mouse models without any side effects compared to live bacteria, suggesting that SE-EVs may to some extent be a substitute for live parental bacteria[25]. However, the application of SE-EVs to treat bacterial infection AD is limited due to the lack of inherent antimicrobial activity. In addition, even endowed with antimicrobial activity, non-selective antimicrobial activity may harm the indigenous skin microbiota[27]. Furthermore, since *S. aureus* is present below the epidermis, topical application of SE-EVs with limited skin permeation ability could not lead to satisfying therapeutic effectiveness[25,28]. Therefore, to achieve effective bacterial infection AD treatment and maintain skin homeostasis, SE-EVs should be equipped with deep skin penetration ability and selective *S. aureus* killing capability.

Microneedle (MN) containing micrometer-sized sharp needles can effectively disrupt the stratum corneum and form transient transdermal delivery microchannels without touching nerve fibers and blood vessels, and thus provide a convenient and pain-free solution to enhance the transdermal delivery efficiency of loaded cargoes[29]. Among various types of MN, dissolving MN, especially HA-based MN, shows advantages of biosafety, convenient administration, high drug loading capacity, and dosing precision, and thus have attracted tremendous research attention for the treatment of cutaneous disorders such as AD and skin infections[30,31]. Besides, studies show that HA contributes to the uninfected AD treatment by alleviating inflammation response and increasing the self-defence of skin epithelium[32,33]. There have been reports that combining EVs (such as mesenchymal stem cell-EVs and curcumin-encapsulated EVs) with dissolving MN can achieve a synergistic effect for enhanced transdermal delivery for the effective promotion of wound healing[34,35].

Hence, inspired by the application of commensal skin bacteria with antimicrobial activity to treat skin disease, we utilized SE-EVs for bacterial infection AD treatment. To achieve the super antimicrobial effect, Lev was encapsulated into SE-EVs to

develop nanoantibiotics (Lev@SE-EVs). This novel Lev@SE-EVs were further incorporated into a hyaluronic acid (HA)-based MN to fabricate a nanoantibiotics-integrated MN delivery platform (termed Lev@SE-EVs@MN) with remarkably improved transdermal delivery efficiency and enhanced epidermal barrier function. The therapeutic potential of Lev@SE-EVs@MN in an ovalbumin (OVA)-sensitization AD mouse model with *S. aureus* infection was investigated. This commensal skin microbiota-derived EVs integrated MN delivery platform exhibited unique therapeutic functions, including modulating epidermal immune responses, selective killing of pathogenic bacteria, and effectively antimicrobial activity while simultaneously ameliorating inflammation (Fig. 1), suggesting a new strategy for effective bacterial infection AD treatment with unique safety.

2. Materials and methods

2.1. Bacteria strains, cell lines, and animals

S. epidermidis (ATCC12228), *S. aureus* (ATCC 25923), *P. acnes* (ATCC6919), and *E. coli* DH5α were purchased from the BeNa Culture Collection (Beijing, China). *S. epidermidis* (ATCC12228), *S. aureus* (ATCC 25923), and *E. coli* DH5α were cultured in Luria−Bertani (LB) (Life-iLab, Shanghai, China) broth or on LB agar plates at 37 °C with/without shaking (200 rpm) by thermostatic shaker (Jiecheng TS-1102C, Shanghai, China). *P. acne* (ATCC6919) was cultured in brain heart infusion (BHI) (Life-iLab) broth or on BHI agar plates under anaerobic conditions.

Immortalized human keratinocyte cells (HaCaT) and human dermal fibroblasts (HDF) were obtained from the ATCC. The murine macrophage cells (RAW264.7) and murine fibroblast cells (L929) were purchased from the BeNa Culture Collection. All cells were maintained in DMEM (Gibco, Waltham, MA, USA) high glucose supplemented with 10% fetal bovine serum (Gibco) at 37 °C in an atmosphere of 5% CO_2 with humidity. The cells were used for further experiments when the confluence reached more than 80% in plates.

All experiments involving live animal work were in accordance with the Guide for the Care and Use of Laboratory Animals of Huazhong University of Science and Technology (Wuhan, China) and approved by the Institutional Animal Ethical Committee of Huazhong University of Science and Technology. For mouse experiments, BALB/c female mice (aged 8 weeks, weight of 20 ± 2 g) and SD rats (male, 200 ± 20 g in weight) were purchased from the Hubei Provincial Center for Disease Control and Prevention (Wuhan, China) and maintained in standard specific pathogen-free conditions at 22 °C under a 12-h light/dark cycle and with free access to water and food.

2.2. Preparation and characterization of Lev@SE-EVs

SE-EVs were obtained according to previous publication[25]. A repeated freeze-anneal-thaw loading method was used to prepare nanoantibiotics Lev@SE-EVs. Briefly, Lev (256 μg/mL; Meilunbio, Dalian, China) dissolved in PBS (Gibco) and SE-EVs solution (7.15×10^{11} particles/mL) were mixed in equal volumes. The mixed solution was performed by three freeze−anneal−thaw cycles (freezing at −196 °C for 5 min, annealing at −1.4 °C for 30 min, and thawing at 65 °C for 10 min), followed by washing with PBS five times by an ultrafiltration tube (MWCO 100 kDa, MilliporeSigma, Burlington, MA, USA) to remove the unencapsulated Lev and obtain Lev@SE-EVs.

The microstructure of Lev@SE-EVs was observed using transmission electron microscopy (H-7000FA, Hitachi, Tokyo, Japan). Size distribution and yield of Lev@SE-EVs were assessed using Nanoparticles Tracking Analysis (NS300, NTA LM-10, Malvern, United Kingdom). To ensure equivalent results, samples were diluted up to 1:1000 or 1:5000 to ensure a concentration of 20−120 particles/frame. A 100 μL sample was placed in the chamber furnished with a green laser. The video was recorded using NanoSight 3.1 with a camera level varying between 13 and 15. Each sample was recorded three times for 30 s and a detection threshold of approximately 5 was used in the calculations to ensure comparable results. The concentration of Lev@SE-EVs is $6.35 \times 10^{11} \pm 8.21 \times 10^{8}$ particles/mL. The size distribution, zeta potential, and PDI of Lev@SE-EVs were measured on a Zetasizer Nano ZS90 (Malvern Instruments, Malvern, United Kingdom). The total protein content of Lev@SE-EVs was determined using a BCA Protein Assay kit (Beyotime, Shanghai, China) according to the manufacturer's instructions. Protein profiles of Lev@SE-EVs were analyzed by SDS-PAGE with 3-Color Prestained Protein Standards (Accurate Biology, Hunan, China). Characterization of SE-EVs and (i)Lev@SE-EVs that Lev@SE-EVs were isolated from Lev@SE-EVs@MN were analyzed through the same procedure.

To measure the drug content, Lev@SE-EVs (6.35×10^{11} particles/mL) were treated with 0.1 mol/L EDTA for 4 h at 37 °C and then centrifuged to remove empty SE-EVs. The Lev concentrations in the supernatant were measured as 1.77017 ± 0.00236 using a microplate reader (Spark, Tecan, Switzerland) at 287 nm

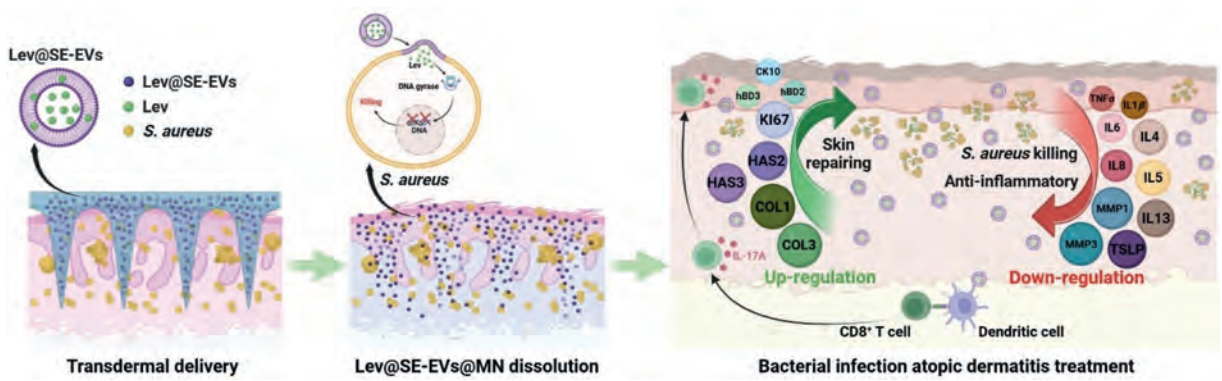

Figure 1 Schematic diagram of MN therapy. The treatment of bacterial infection atopic dermatitis through antibacterial, anti-inflammatory, and skin repair.

and calculated with the reference standard curve ($y = 0.0057x + 1.3696$, $R^2 = 0.9991$) using serial dilutions of free Lev (0−256 μg/mL). According to the following standard curve, the Lev concentration in the supernatant is 70.27 ± 0.42 μg/mL. According to a similar prior report[36], the content of drug loading (μg/10^{11} particles) was calculated according to the ratio of the content of encapsulated Lev to the total number of SE-EVs particles, namely, the content of Lev loading (μg/10^{11} particles) = (70.27 ± 0.42 μg/mL)/(6.35 × 10^{11} particles/mL) = 11.07 ± 0.07 μg/10^{11} particles. To investigate the antibiotic stability in Lev@SE-EVs, Lev, and Lev@SE-EVs solutions were stored at −80 °C, −20 °C and 4 °C in the dark for 25 days or under continuous exposure with white light (WL) for 25 days or ultraviolet (UV) light at room temperature (RT) for 25 h, and then treated with EDTA to analyze the content of Lev in the SE-EVs.

In vitro Lev release from Lev@SE-EVs was determined using a dialysis method. 2 mL of Lev@SE-EVs (6.35 × 10^{11} particles/mL) dispersed in PBS (pH 7.4 or pH 4.0) was added into a dialysis bag (MWCO 14 kDa, Biosharp, Hefei, China). The dialysis bags were immersed into a centrifuge tube containing 6 mL of release buffer (PBS, pH 7.4 or pH 4.0), respectively, and immediately incubated at 37 °C with shaking at 150 rpm in the darkness. The release buffer was collected at certain time points and immediately replaced with equivalent fresh release medium. The collected sample was detected for drug content using a microplate reader at 287 nm.

2.3. Preparation and characterization of Lev@SE-EVs@MN patches

To load the MN with Lev@SE-EVs, 4 g of sodium hyaluronate (88 kDa, Freda Biochem Co., Ltd., China) was dissolved in 4 mL of Lev@SE-EVs (9.92 × 10^9 particles/mL) solution and stirred until completely dissolved. The resulting solution was left overnight at 4 °C to remove the bubbles. The polydimethylsiloxane MN mold with a pyramidal needle shape (10 × 10 arrays, with needle height of 620 μm and a base diameter of 300 μm; Taizhou Microchip Medical Technology Co., Ltd., China) was vacuumed for 5 min, added with 200 μL of the resulting solution, centrifuged and dried at room temperature for 24 h to obtain the Lev@SE-EVs@MN patches. For the preparation of the blank MN patches, the MN patches loaded with Lev (Lev@MN), the MN patches loaded with SE-EVs (SE-EVs@MN), the MN patches loaded with DiI-stained Lev@SE-EVs (Lev@SE-EVs@DiI@MN) and the MN patches loaded with methylene blue (MB; MB@MN), Lev@SE-EVs solution was replaced with PBS, Lev (4 μg/mL), SE-EVs (9.92 × 10^9 particles/mL), DiI-stained SE-EVs (9.92 × 10^9 particles/mL) or MB (0.8%, *w/v*) solution in the first step, followed by the same protocol as described before.

The microstructure of MN patches was observed by FESEM (Sirion 200, Netherlands), industrial CCD video microscope (Renyue, Shanghai, China), and confocal laser scanning microscopy (CLSM) (Olympus, Tokyo, Japan). The mechanical strengths of MN patches were detected by a universal mechanical testing machine (Sunstest, Shenzhen, China). To test the skin insertion capacity, MB@MN was inserted into the excised skin of the mouse for 10 min and then the backing layer was discarded and the Lev@SE-EVs@MN array was tested by a parafilm M® model that six layers of parafilm M® were used to simulate the thickness of the excised skin. The skin and each membrane of parafilm M® were imaged by a stereoscopic microscope (SteREO Discovery. V8, Carl Zeiss, Germany). To assess the penetration depth, Lev@SE-EVs@DiI solution and Lev@SE-EVs@DiI@MN were applied to the porcine skin of SD rats for 15 and 120 min. The treated skin was washed, quick-frozen by liquid nitrogen, embedded in the optimal cutting temperature compound, and sliced at a thickness of 10 μm by a cryostat microtome (HM5525NX, Thermo Fisher Scientific, Waltham, MA, USA). Then, skin cross-sections were visualized by CLSM. To investigate the solubility, the Lev@SE-EVs@MN were inserted into the excised mouse skin for 0, 2, 5, 10, or 15 min. Afterward, the MN was peeled off, dried overnight at room temperature, and imaged with an optical microscope (Leica, Wetzlar, Germany).

2.4. Biocompatibility of Lev@SE-EVs and Lev@SE-EVs patches

The biocompatibility of Lev@SE-EVs was analyzed by the cell viability and the acute toxicity. The cell viability of Lev@SE-EVs was performed by the CCK-8 method. Briefly, HaCaT, HDF, RAW264.7, and L929 cells (1 × 10^5 cells/well) were seeded into 96-well plates for 24 h, respectively. The samples containing SE-EVs or Lev@SE-EVs (3 × 10^2−3 × 10^5 particles/cell) were prepared in the culture medium. PBS was used as a negative control. The cells were treated with the samples for 24 h and then analyzed by CCK-8 kits (Sparkjade, China) according to the manufacturer's instructions. In addition, the acute toxicity of Lev@SE-EVs was analyzed in BALB/c female mice. A 10-fold concentration (9.92 × 10^{10} particles/mL) of SE-EVs or Lev@SE-EVs was administered to mice by gavage or applied topically to the back of mice for 28 consecutive days. The mice were monitored every 7 or 14 days for changes in body weight, transepidermal water loss (TEWL), corneometer, and erythema. On Day 28, the liver, spleen, heart, lung, kidney, and dorsal skin were harvested and stained with hematoxylin and eosin (H&E). Furthermore, the mouse ears were applied topically by a concentration (9.92 × 10^9 particles/mL) of SE-EVs or Lev@SE-EVs and then were digested to obtain single-cell suspensions for further FACS analysis.

The biocompatibility of Lev@SE-EVs patches was conducted by hemolysis assay test. Fresh red blood cells (RBCs) were obtained by centrifuge at 4500 rpm for 10 min at 4 °C. RBCs were washed with saline three times and were diluted up to 1:20. 500 μL of different samples were separately added to 500 μL of RBC suspensions. Deionized water was used as a positive control and saline was used as a negative control. After incubation at 37 °C for 2 h, the solution was centrifuged 4500 rpm for 10 min at 4 °C. The hemolytic activity was determined by a microplate reader at 570 nm. The rate of hemolysis was calculated by Eq. (1):

$$\text{Rate of hemolysis } (\%) = [(OD_{sample} - OD_{negative})/(OD_{positive} - OD_{negative})] \times 100 \quad (1)$$

2.5. In vitro bacterial killing assay of Lev@SE-EVs and (i) Lev@SE-EVs

The antimicrobial effect of Lev@SE-EVs on *S. aureus* was analyzed by using serial dilutions. Briefly, after Lev@SE-EVs (7.94 × 10^{10} particles/mL) were serially diluted with sterile PBS, 100 μL different concentrations of Lev@SE-EVs were added to a 96-well plate. Sterile PBS was used as a negative control. Then 100 μL of *S. aureus* suspension adjusted to 10^5 CFU/mL using fresh LB culture was added to the plate. The plate was incubated at 37 °C in a microplate reader, with OD_{600} measured every 30 min for 16 h to obtain the growth curves of *S.*

aureus. A dose−response curve of Lev@SE-EVs to *S. aureus* was calculated. The antimicrobial effect of (i)Lev@SE-EVs on *S. aureus* was analyzed by the same method. Briefly, Lev@SE-EVs@MN patches were cut up and then dissolved in PBS. The mixture is centrifuged to obtain (i)Lev@SE-EVs. The antimicrobial effect of (i)Lev@SE-EVs was performed according to the above description.

2.6. *Uptake assessment of SE-EVs and Lev@SE-EVs*

SE-EVs and Lev@SE-EVs were used for cellular uptake in *S. epidermidis*, *S. aureus*, *P. acnes,* and *E. coli*. The growth curves of different bacteria were measured by incubating 100 μL (10^5 CFU/mL) of bacterial suspension with 100 μL of SE-EVs at various concentrations (1.98×10^{10}, 9.92×10^9 or 4.96×10^9 particles/mL) in a

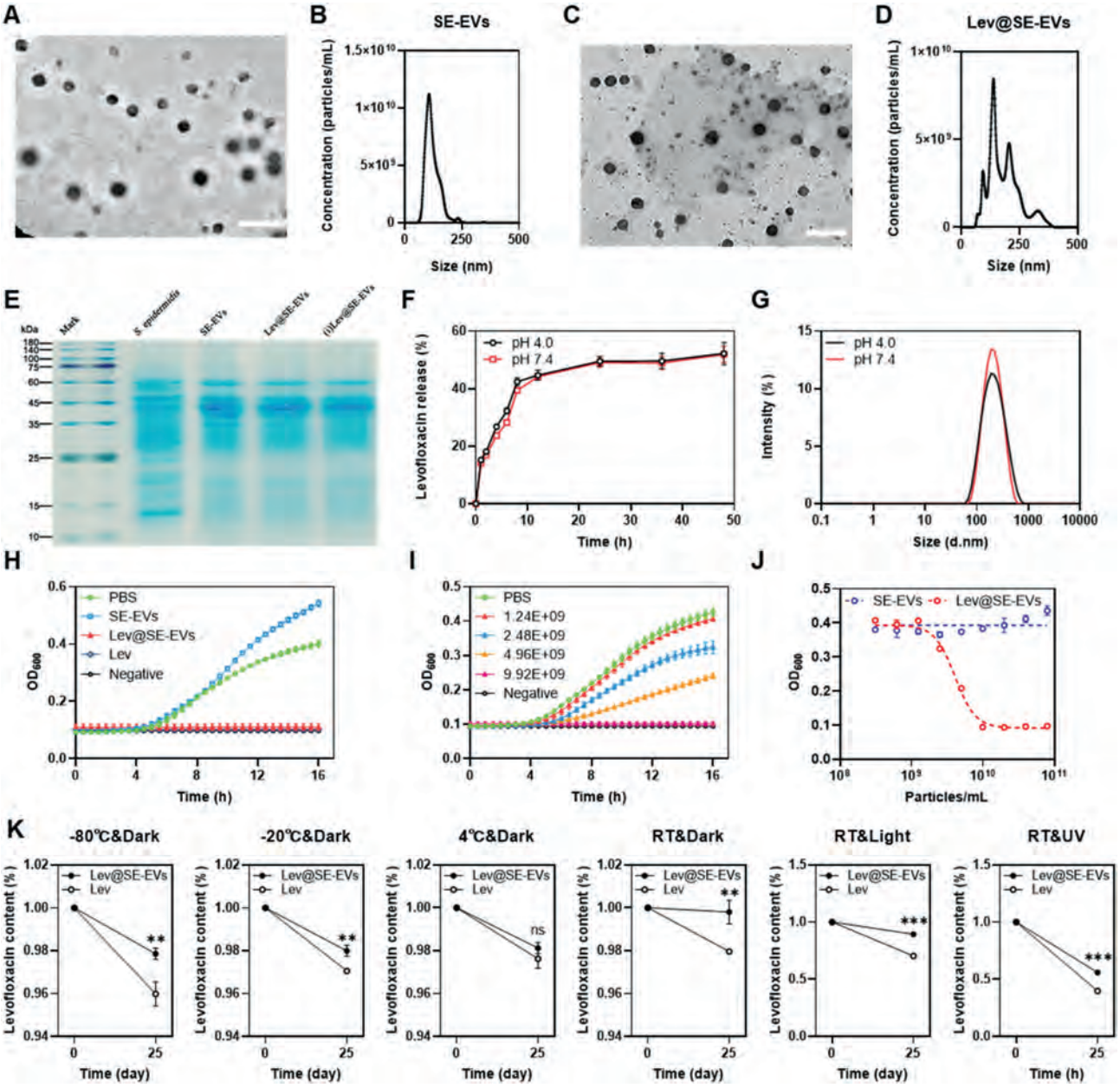

Figure 2 Characterization of Lev@SE-EVs. (A−D) Transmission electron microscopy images of SE-EVs (A) and Lev@SE-EVs (C), and nanoparticle tracking analysis of averaged spectra of the size distribution of SE-EVs (B) and Lev@SE-EVs (D). Scale bar = 1 μm. (E) SDS-PAGE analysis of the protein profiles of *S. epidermidis*, SE-EVs, Lev@SE-EVs, and (i)Lev@SE-EVs. (F) Release profiles of Lev from Lev@SE-EVs (6.35×10^{11} particles/mL) dispersed in PBS at pH 4.0 or pH 7.4 ($n = 3$). (G) Dynamic light scattering analysis of the particle size of Lev@SE-EVs at pH 4.0 and pH 7.4. (H) Growth curves of *S. aureus* cultured with PBS, SE-EVs (6.35×10^{11} particles/mL), Lev@SE-EVs (6.35×10^{11} particles/mL), and Lev (MIC 4 μg/mL) for 16 h ($n = 3$). (I) Growth curves of *S. aureus* incubated with different concentrations of Lev@SE-EVs ($n = 3$). (J) Dose−response curve of Lev@SE-EVs or SE-EVs by incubating increasing concentrations of Lev@SE-EVs or SE-EVs with *S. aureus* ($n = 3$). (K) The activity rates of free Lev and Lev inside Lev@SE-EVs when stored at −80 °C, −20 °C, 4 °C, and room temperature (RT) under the dark or at RT under the light or UV. Data are reported as the mean ± SD. $^{***}P < 0.001$ and $^{**}P < 0.01$ as determined by Student's *t* test and one-way ANOVA. (i)Lev@SE-EVs, isolated Lev@SE-EVs from Lev@SE-EVs@MN. ns, no significance.

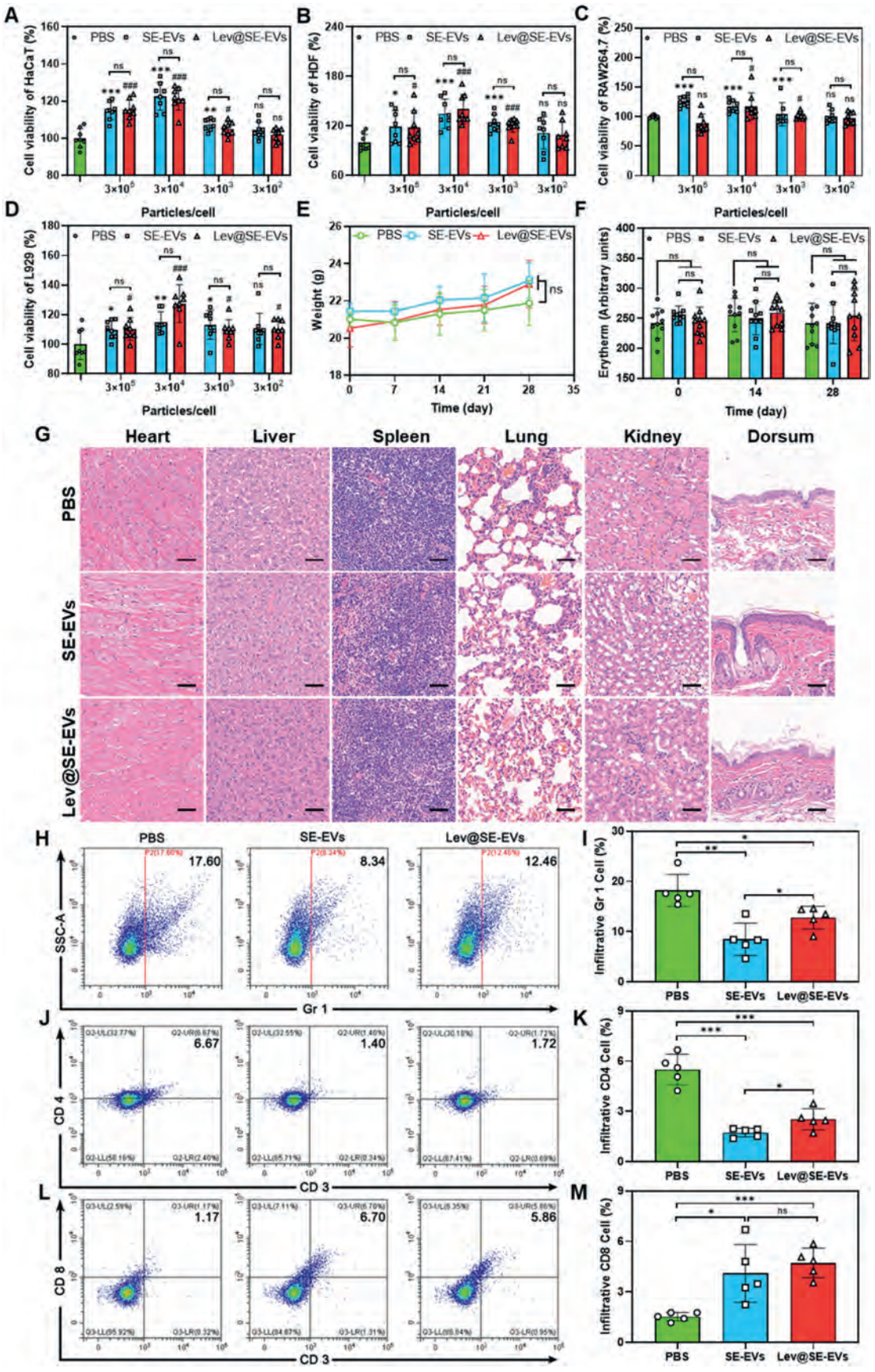

Figure 3 Biocompatibility and epidermal immune responses of Lev@SE-EVs. (A−D) Cell viability of various cells (HaCaT, HDF, RAW264.7, and L929 cells) incubated with Lev@SE-EVs or SE-EVs at the dose of 3×10^2−3×10^5 particles per cell for 24 h ($n = 8$). (E) The body weight

96-well plate. The plate was incubated at 37 °C in a microplate reader, and the OD_{600} was measured at the indicated time points. PBS was used as a control. SE-EVs or Lev@SE-EVs were stained with 0.1 wt% DiI, followed by washing with PBS three times with an ultrafiltration tube (MWCO 100 kDa, MilliporeSigma) to remove the unbound dye. After incubating bacteria suspensions (10^9 CFU/mL) with 6.35×10^{11} particles of SE-EVs@DiI or Lev@SE-EVs@DiI for 2 h, the bacteria suspensions were centrifuged at 3000×*g* for 5 min to remove unuptaken SE-EVs@DiI or Lev@SE-EVs@DiI. The bacteria pellets were dispersed in PBS and were used to analyze the uptake efficiency of SE-EVs@DiI or Lev@SE-EVs by flow cytometer. Flow cytometric analysis was performed using FlowJo software. In addition, the bacteria pellets were stained with 1 μg/mL DAPI nucleic acid at 37 °C for 10 min. After centrifugation at 3000×*g* for 5 min to remove excess dye, the bacteria pellets were dispersed in PBS and imaged by CLSM.

2.7. Analysis of skin microbiota after topical SE-EVs application

Mouse-ear skin was topically applied by SE-EVs (9.92×10^9 particles/mL) once a day for 28 consecutive days. Mouse-ear skin microbiota samples were obtained before and after application as described previously[37]. In brief, the ear skin of mice was swabbed with a sterile cotton swab previously soaked in a solution of 0.15 mol/mL NaCl and 0.1% Tween 20 for 50 times. The swabs were snap-frozen and stored at −80 °C immediately after collection. Bacterial DNA was extracted from swabs as reported[38]. The V3−V4 hypervariable regions of the bacteria 16S rRNA gene were amplified with primers 338F (5′-ACTCCTACGGGAGGCAGCAG-3′) and 806R (5′-GGACTACHVGGGTWTCTAAT-3′) by thermocycler PCR system (GeneAmp 9700, ABI, USA). PCR products were purified using the AxyPrep DNA Gel Extraction Kit (Axygen Biosciences, Union City, CA, USA) and quantified according to the Illumina Miseq platform (Illumina, San Diego, USA) Standard Operating Procedures. Approximately equivalent amounts of purified amplicons were pooled in equimolar and paired-end sequenced (2 × 300) on an Illumina MiSeq platform (Illumina, San Diego, USA) following the standard protocol. Sequencing data were analyzed according to report[39].

2.8. Mice treatment

AD was induced by repeated epicutaneous sensitization of tape-stripped skin with OVA, followed by infection with *S. aureus*, as described previously with slight modifications[38]. Briefly, mouse dorsal skin was tape-stripped with 3M adhesive tape (10 times/tape). After 24 h, 1 mg/mL OVA solution was applied on the tape-stripped dorsal skin of mice by a skin swab for 7 consecutive days. Mice received three 7-day OVA treatments at 2-week intervals. 24 h at the end of OVA treatment, mice were tape-striped to simulate mechanical skin damage caused by scratching. *S. aureus* suspended in PBS (10^7 CFU/mL) was painted on the back of mice. After 4 h, mice were topically applied with commercial Lev product, SE-EVs, Lev@SE-EVs, blank MN, Lev@MN, SE-EVs@MN, or Lev@SE-EVs@MN for 14 consecutive days, wherein a total of 0.2 mL of Lev, SE-EVs, and Lev@SE-EVs were painted by a sterile swab. At the end of Week 10, corneometer, erythema, and TEWL of mouse dorsal skin were detected by a Tewameter TM300, Corneometer CM825, and Mexameter MX18 (C & K, Germany) in 50% ambient humidity at 20 °C, respectively. The scratching frequency of mice was monitored for 30 min. Blood samples were obtained by removing the eyeball to analyze the levels of IgE *in vivo* with ELISA kits (Jonlnbio, Shanghai, China) according to the standard instructions. Mouse dorsal skin was collected by a disposable 6 mm-diameter skin biopsy punch, either fixed with paraformaldehyde for histology and immunofluorescence analysis, rapidly frozen for RNA extraction, homogenized for CFU counting, or digested to get single-cell suspensions for FACS analysis.

2.9. Histology and immunofluorescence analysis

The mouse dorsal skin or mouse ear was fixed in 4% formaldehyde, embedded in paraffin, and sectioned at 5 μm. For histological analysis, the sections were stained with H&E. For immunofluorescence analysis, the sections were deparaffinized, rehydrated, and blocked. The primary antibodies used are anti-CD8 (Abcam), anti-IL-17A (Abcam), anti-CK10 (Abcam), anti-Ki67 (Abcam) and, anti-lipoteichoic acid (LTA) antibodies (Invitrogen, Carlsbad, CA). Secondary antibodies used are goat anti-rabbit IgG and Alexafluor conjugated 647 goat anti-rabbit lgG (Abcam) or Alexafluor conjugated 647 goat anti-rabbit lgG (Abcam). After the tissue was stained with DAPI, the images were analyzed by CLSM.

2.10. Quantitative real-time PCR

After incubation with PBS or dead *S. aureus* (10^7 CFU/mL) that was killed by UV, cells were treated with different samples. The total RNA of cells was extracted after different stimulations by the RNA extraction solution (Servicebio, Wuhan, China) and reverse transcribed by the ServicebioRT First Strand cDNA Synthesis Kit (Servicebio). The quantitative real-time PCR was conducted using 2 SYBR Green qPCR Master Mix (None ROX, Servicebio) by the BioRad CFX96 Touch System. The PCR primer sequences are listed in Supporting Information Table S2. RNA expression levels were normalized by the *GAPDH* housekeeping gene in each sample. The fold change of gene expression levels was analyzed by the comparative $2^{-\Delta\Delta CT}$ method. All the assays were performed in triplicate. The total RNA of skin tissues was analyzed by the same procedure.

2.11. CFU counting

Mouse dorsal skin was punched by a disposable 6 mm-diameter skin biopsy punch. Tissues were measured for thickness by a

of mice treated with Lev@SE-EVs or SE-EVs by oral gavage at a dose of 9.92×10^{10} particles/mL for 28 consecutive days ($n = 5$). (F) The erythema on the dorsal skin of mice treated with Lev@SE-EVs or SE-EVs by topical application at a dose of 9.92×10^9 particles/mL for 28 consecutive days ($n = 10$). (G) H&E staining of the heart, liver, spleen, lung, kidney, and dorsal skin of the mice on Day 28. Scale bar = 50 μm. (H−M) Flow cytometry analysis and corresponding quantitative analyses of $Gr1^+$ cell, $CD4^+$ T cell, and $CD8^+$ T cell populations in mouse ears after treatment with Lev@SE-EVs or SE-EVs at a dose of 9.92×10^9 particles/mL for 28 consecutive days ($n = 5$). Data are reported as the mean ± SD. ***$P < 0.001$, **$P < 0.01$, and *$P < 0.05$ as determined by Student's *t* test and one-way ANOVA. ns, no significance.

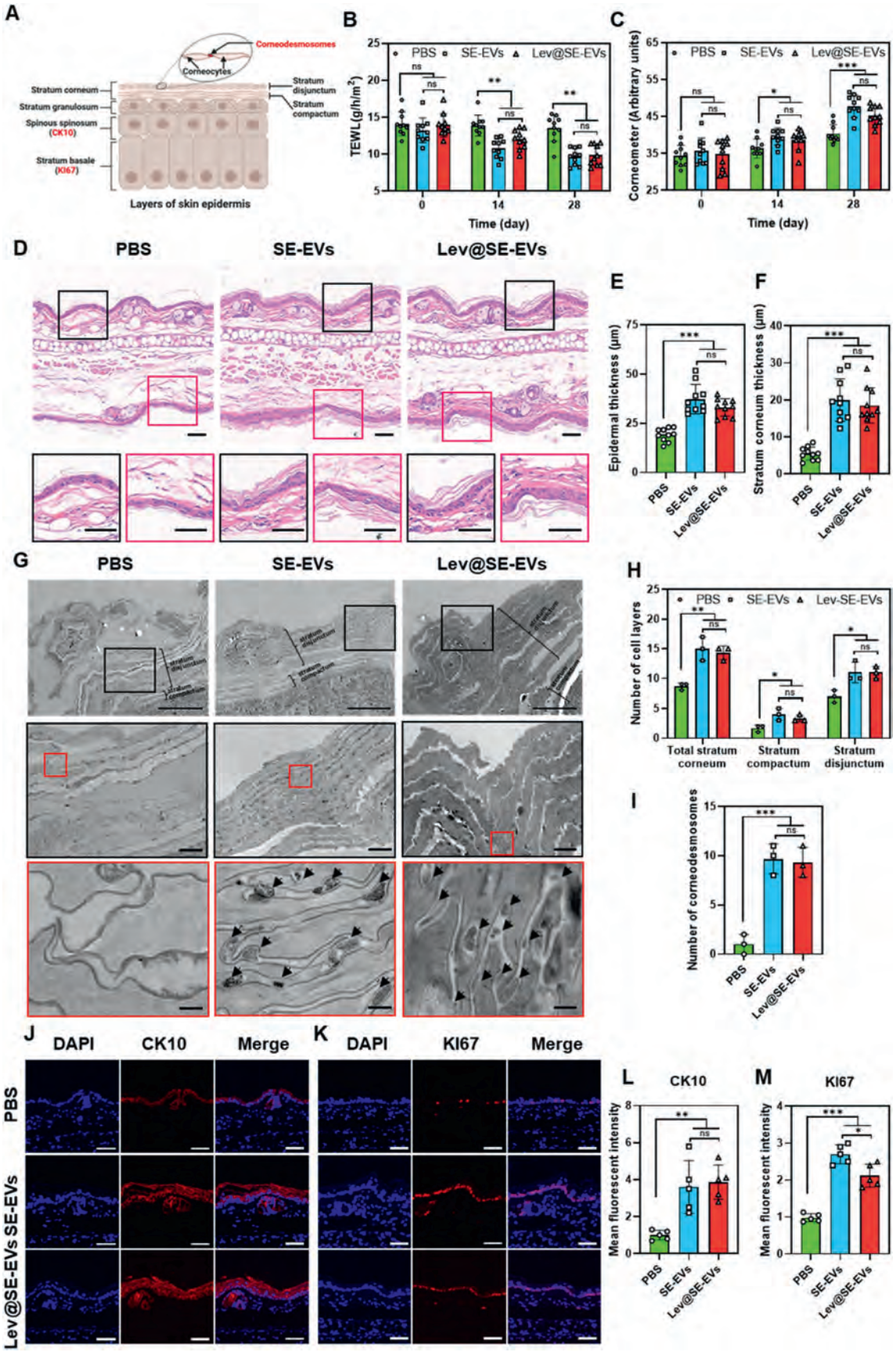

Figure 4 Lev@SE-EVs enhance epidermal barrier function. (A) Schematic depiction of the stratum corneum layers and epidermis layers for understanding histopathology and ultrastructural analysis. (B, C) The TEWL (B) and corneometer (C) of mouse ears were treated with Lev@SE-

micrometer, and loaded into a centrifuge tube containing 500 μL sterile water and 2 ceramic beads with a diameter of 0.5 mm. Tissue was homogenized with bead beating for 3 min at 70 Hz and CFUs were counted by serial dilution on LB agar plates after 36 h incubation at 37 °C. Both *S. aureus* and total bacterial colonies were counted and normalized to volumes of tissues. *S. aureus* colonies were visible as yellow colonies that could be discriminated against total bacteria and were further identified by 16S rDNA.

2.12. Flow cytometry analysis of mouse skin tissues

Mouse skin tissues (mouse ears or mouse dorsal skin) were collected after different treatments. Mouse skin tissues were cut into pieces and then incubated in high-glucose DMEM culture medium containing DNase I (1 mg/mL; Solarbio, Beijing, China) and collagenase IV (2 mg/mL; Biosharp, Hefei, China) for 2 h at 37 °C to obtain single-cell suspensions. Cells were blocked with anti-CD16/32 antibody (BioLegend, San Diego, CA) and then stained with APC anti-CD3 (clone 17A2, BioLegend), FITC anti-CD4 (clone RM4-5, BD Pharmingen, San Diego, CA), and PE anti-CD8 (clone 53−6.7, BioLegend) for 30 min on ice. The fluorescence of antibodies was analyzed using CytoFlex flow cytometry (FC 500, Beckman Coulter, Brea, CA).

2.13. Cell proliferation and migration of DSA-treated HDF

The proliferation ability of Lev@SE-EVs@MN on DSA-HDF cells was evaluated by EdU assay. Briefly, HDF cells were seeded in 35 mm dishes for 24 h and then pre-treated with DSA for 4 h. After treatment with different samples for 24 h, cell proliferation was performed by the YF®488 Click-iT EdU Universal Cell Proliferation Detection Kit (US EVERBIGHT, Suzhou, China) according to the manufacturer's protocols. The cell nuclei were stained with 0.1 wt% DAPI. The EdU rate was determined by the National Institutes of Health Image J software (Macintosh, Cupertino, CA). The migration effect of Lev@SE-EVs@MN on DSA-HDF cells was performed by scratch wound assay. A confluent layer of HDF cells was scratched using the Culture-Insert (Ibidi, Martinsried, Germany). After pre-treatment with DSA for 4 h, HDF cells were treated with different samples for 24 h. At 0, 12, and 24 h, images were obtained using the microscope. The decrease in the wound area was quantitated by the National Institutes of Health Image J software.

2.14. Western blot

Lysate preparation, gel electrophoresis, and immunoblotting were conducted in accordance with standard protocols. The primary antibodies including anti-COL-I and anti-COL-III (Univ, Shanghai, China) were used. The detection was conducted after incubating with horseradish peroxidase-conjugated secondary antibody and goat anti-mouse IgG (Univ). The chemiluminescent intensity was quantified by the Quantity One software.

2.15. Statistical analysis

The obtained results are expressed as the mean ± standard deviation (SD). GraphPad Prism 8.0 (GraphPad Software, San Diego, CA) was used to perform Student's *t* test or one-way ANOVA. $P < 0.05$ was considered statistically significant.

3. Results

3.1. Characterization of Lev@SE-EVs

In this study, SE-EVs were collected according to our previous publication[25] and then loaded with Lev by repeated freeze-anneal-thaw methods[40]. As shown in Fig. 2A−D, SE-EVs and Lev@SE-EVs displayed a regular spherical structure with a heterogeneous size distribution, with the particle size increased from 121.2 ± 2.1 to 185.3 ± 13.2 nm upon the Lev loading. The polydispersity index (PDI) and zeta potential of SE-EVs and Lev@SE-EVs were 0.256 ± 0.010 and −31.86 ± 3.81 mV, and 0.284 ± 0.016 and −34.56 ± 2.61 mV (Supporting Information Table S1), respectively. There was no difference in protein profiling between SE-EVs and Lev@SE-EVs (Fig. 2E). In addition, the antibiotic content in Lev@SE-EVs was 11.07 ± 0.07 μg/10^{11} particles (The encapsulation efficiency of Lev: 28.62 ± 1.5%). Considering the differences in pH between the normal skin and AD lesional skin[30], the effect of pH on the Lev release from Lev@SE-EVs was inversitaged. Almost no difference in the release efficiency (Fig. 2F) and the particle size (Fig. 2G) was observed between pH 4.0 and pH 7.4, suggesting the release profile and particle size of Lev@SE-EVs were not affected by the skin environmental pH.

Next, the antibacterial effect of Lev@SE-EVs was evaluated. As shown in Fig. 2H, compared with *S. aureus* treated with PBS, SE-EVs did not exhibit a bactericidal effect against *S. aureus*, whereas Lev@SE-EVs show a strong inhibitory effect on *S. aureus*. The inhibitory effect of Lev@SE-EVs was consistent with free Lev at MIC concentrations of 4 μg/mL. To further investigate this effect, *S. aureus* was incubated with various concentrations of Lev@SE-EVs. As shown in Fig. 2I, Lev@SE-EVs concentration at no less than 9.92×10^9 particles/mL was necessary to achieve the inhibition effect against *S. aureus* growth, which was consistent with a typical sigmoidal dose−response curve (Fig. 2J). Notably, the Lev concentration in Lev@SE-EVs at 9.92×10^9 particles/mL was 1.10 μg/mL, which was lower than the MIC concentration (4 μg/mL) of free Lev. These results indicate that loading antibiotics into SE-EVs could enhance the antibacterial efficacy of antibiotics, thus decreasing the dose of antibiotics.

The protective effects of SE-EVs on the stability of the loaded Lev were further explored. As seen in Fig. 2K, although the activities of free Lev and Lev inside Lev@SE-EVs were above 95%

EVs or SE-EVs by topical application at a dose of 9.92×10^9 particles/mL for 28 consecutive days ($n = 10$). (D) H&E staining of mouse ears on Day 28. Scale bar = 50 μm. (E, F) The thickness of epidermis layers (E) and stratum corneum layers (F) in H&E-stained tissue sections from different groups on Day 28 ($n = 10$). (G) Transmission electron microscopy images of glutaraldehyde-fixed mouse ear tissue from different groups on Day 28. Corneodesmosomes (black arrows) represent junctions between the peripheral ends of corneocytes. Scale bars of top to bottom = 10 μm, 2 μm, and 200 nm. (H, I) Corresponding quantitative analyses of the number of cell layers (H) and corneodesmosomes (I) in the stratum corneum ($n = 3$). (J−M) Immunofluorescence-based detection and corresponding quantitative analyses of differentiation marker cytokeratin-10 (CK10) and proliferation marker KI67 in mouse ears from different groups on Day 28 ($n = 5$). Scale bar = 10 μm. Data are reported as the mean ± SD. ***$P < 0.001$, **$P < 0.01$, and *$P < 0.05$ as determined by Student's *t* test and one-way ANOVA. ns, no significance.

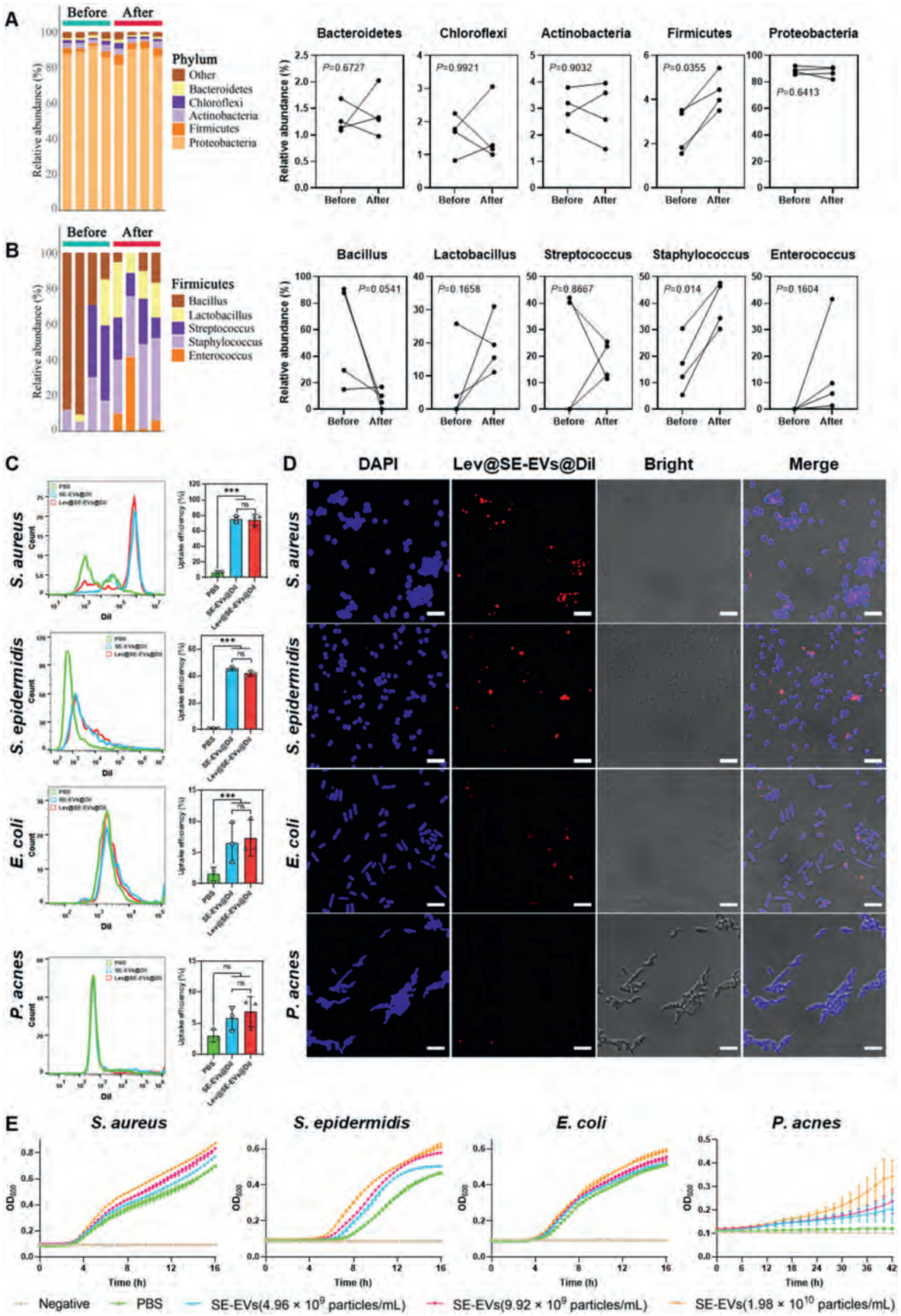

Figure 5 Lev@SE-EVs can be efficiently uptaken by bacteria. (A) Mean relative abundance of the five most prominent phylum in the mouse ears before/after the application of SE-EVs at a dose of 9.92×10^9 particles/mL for 28 consecutive days ($n = 3$). (B) Mean relative abundance of

during storage at −80 °C, −20 °C, 4 °C and room temperature in the dark for 25 days, the activity of Lev in Lev@SE-EVs was slightly higher than that of free Lev. Under natural light exposure at room temperature for 25 days, the activities of free Lev and Lev in Lev@SE-EVs were approximately 70% and 89%, respectively. Similarly, under UV irradiation for 25 h, the activities of free Lev and Lev in Lev@SE-EVs were approximately 39% and 56%, respectively. These results demonstrate that SE-EVs encapsulation could enhance drug stability. In addition, the changes of physical properties (size distribution, PDI, and zeta potential) of Lev@SE-EVs were negligible when stored at −20 °C in the dark (Table S1), suggesting a valuable storage method to maintain Lev@SE-EVs stability.

3.2. Lev@SE-EVs are biocompatible and can regulate epidermal immune responses

The cytotoxicity of Lev@SE-EVs was first investigated *in vitro*. *In vitro* cell viability assays on HaCaT, HDF, RAW264.7, and L929 cells show that Lev@SE-EVs were nontoxic and promoted the proliferation of these cells compared to the PBS group (Fig. 3A−D). The biocompatibility of Lev@SE-EVs was further assessed *in vivo*. Mice were treated with Lev@SE-EVs through oral gavage and topical administration on the back for 28 consecutive days. Compared to the PBS group, no significant change in body weight, erythema, and pathogenic was observed in the Lev@SE-EVs group (Fig. 3E−G). On the basis of previous findings that SE-EVs activate an initial immune response[25], the immune response induced by Lev@SE-EVs should be considered. Therefore, the immune response of Lev@SE-EVs in epidermal cells and mouse ears was investigated. Lev@SE-EVs induced the expression of human β-defensin (*hBD*) 2 and *hBD*3 in HaCaT cells in a time-dependent manner but not *CAMP* in HaCaT cells (Supporting Information Fig. S1A−S1C). Topical application of Lev@SE-EVs decreased the abundances of $CD4^+$ T cells and $Gr1^+$ cells (Fig. 3H−K) but increased $IL17A^+$ $CD8^+$ T cells (Fig. 3L and M; Fig. S1D) in normal mice. Similar results were also observed in SE-EVs (Fig. 3A−M, Fig. S1A−S1D). These results indicate that Lev@SE-EVs had good biocompatibility and regulated epidermal immune responses.

3.3. Lev@SE-EVs enhance epidermal barrier function

The well-functioning stratum corneum tightly maintains the moisture concentration gradient in the skin, allowing moisture to passively diffuse from the inner to the outer layers[38]. Epidermal barrier damage impairs the ability of the stratum corneum to control this moisture concentration gradient, leading to an increase in TEWL (a fully established method for assessing epidermal barrier disruption)[41]. Low TEWL values indicate that the skin is intact and reduced TEWL is associated with an enhanced epidermal barrier (Fig. 4A). To validate the role of the Lev@SE-EVs on the epidermal barrier *in vivo*, mouse ears were topically applied with Lev@SE-EVs for 28 consecutive days. Compared to the PBS group, considerably reduced TEWL, elevated corneometer, and increased thickness of the epidermis and stratum corneum were observed in the Lev@SE-EVs group (Fig. 4B−F), suggesting that Lev@SE-EVs effectively enhanced epidermal barrier function. The molecular mechanism was further explored. As shown in Fig. 4G−I, compared to the PBS group, a greater number of the stratum corneum monolayers was noted in the Lev@SE-EVs group, with a more prevalent pattern showing the stratum disjunctum layers to be almost interconnected by corneodesmosomes (black arrows) at the outer edges of corneocytes. In addition, immunofluorescence analysis of molecular biomarkers showed that Lev@SE-EVs markedly increased expression of cytokeratin-10 (CK10) and KI67 in normal mouse skin (Fig. 4J−M), implicated in epidermal barrier integrity and epidermal cell renewal. Similar results were observed in SE-EVs (Fig. 4B−M). Altogether, these findings suggest that Lev@SE-EVs remarkably enhanced epidermal barrier function.

3.4. Lev@SE-EVs can be efficiently uptaken by bacteria

EVs play an important role in bacterial intraspecific and interspecific communication. To assess the impact of SE-EVs on the skin microbiota, SE-EVs were topically applied to the ear skin of normal mice once a day for 28 consecutive days and the relative abundances of the most prominent taxa were compared before/after the application of SE-EVs. As shown in Fig. 5A, of the five most prominent phylum in the mouse ears, only *Firmicutes* was significantly increased after application (4.32 ± 0.82%) compared to before application (2.57 ± 1.02%, $P = 0.0355$). Furthermore, of the top five genera in *Firmicutes* (Fig. 5B), only the relative abundance of *Staphylococcus* was significantly increased after application (39.67% ± 8.63%) compared to before application (16.34 ± 10.59%, $P = 0.014$). However, differences in *Bacillus*, *Lactobacillus*, *Streptococcus,* and *Enterococcus* relative abundances between before and after application were not statistically significant. These results suggest that SE-EVs could regulate the level of the *Staphylococcus* genus among skin microbiota.

Whether SE-EVs could selectively interact with specific bacterial genera among the skin microbiota was further explored. As shown in Fig. 5C, the proportions of SE-EVs uptaken by *S. aureus* and *S. epidermidis* were 75.16 ± 4.03% and 45.41 ± 1.43%, respectively, while the proportions of SE-EVs uptaken by *E. coli* and *P. acnes* were only 6.59 ± 3.23% and 5.8 ± 1.93%, respectively. These results suggest that SE-EVs could be preferentially taken up by specific genera. *S. aureus* and *S. epidermidis* were classified as *Staphylococcus* genus. Notably, the cellular uptake of SE-EVs was higher in *S. aureus* than in *S. epidermidis*, indicating that the uptake level varied from species within the *Staphylococcus genus*. Most importantly, there was no significant change in cellular uptake by different bacteria between SE-EVs and Lev@SE-EVs, suggesting that loading Lev into SE-EVs did not affect bacterial cellular uptake of Lev@SE-EVs. In addition, the cellular uptake of SE-EVs and Lev@SE-EVs by different bacteria was qualitatively shown by confocal laser scanning microscopy (CLSM; Fig. 5D; Supporting Information Fig. S2). The effects of SE-EVs cellular uptake on bacterial growth were further investigated. As shown in Fig. 5E, SE-EVs markedly promoted the growth of *S. aureus* and *S. epidermidis* in a concentration-

the top five genera in Firmicutes ($n = 3$). (C) Flow cytometry analysis of the proportions of DiI@Lev@SE-EVs or DiI@SE-EVs that were uptaken by different bacteria for 2 h ($n = 3$). (D) CLSM images of DiI@Lev@SE-EVs uptaken by different bacteria at Hour 2. Scale bar = 5 μm. (E) Growth curves of different bacteria incubated with SE-EVs at a dose of 4.96×10^9, 9.92×10^9 or 1.98×10^{10} particles/mL ($n = 3$). Data are reported as the mean ± SD. ***$P < 0.001$ as determined by Student's t test and one-way ANOVA. ns, no significance.

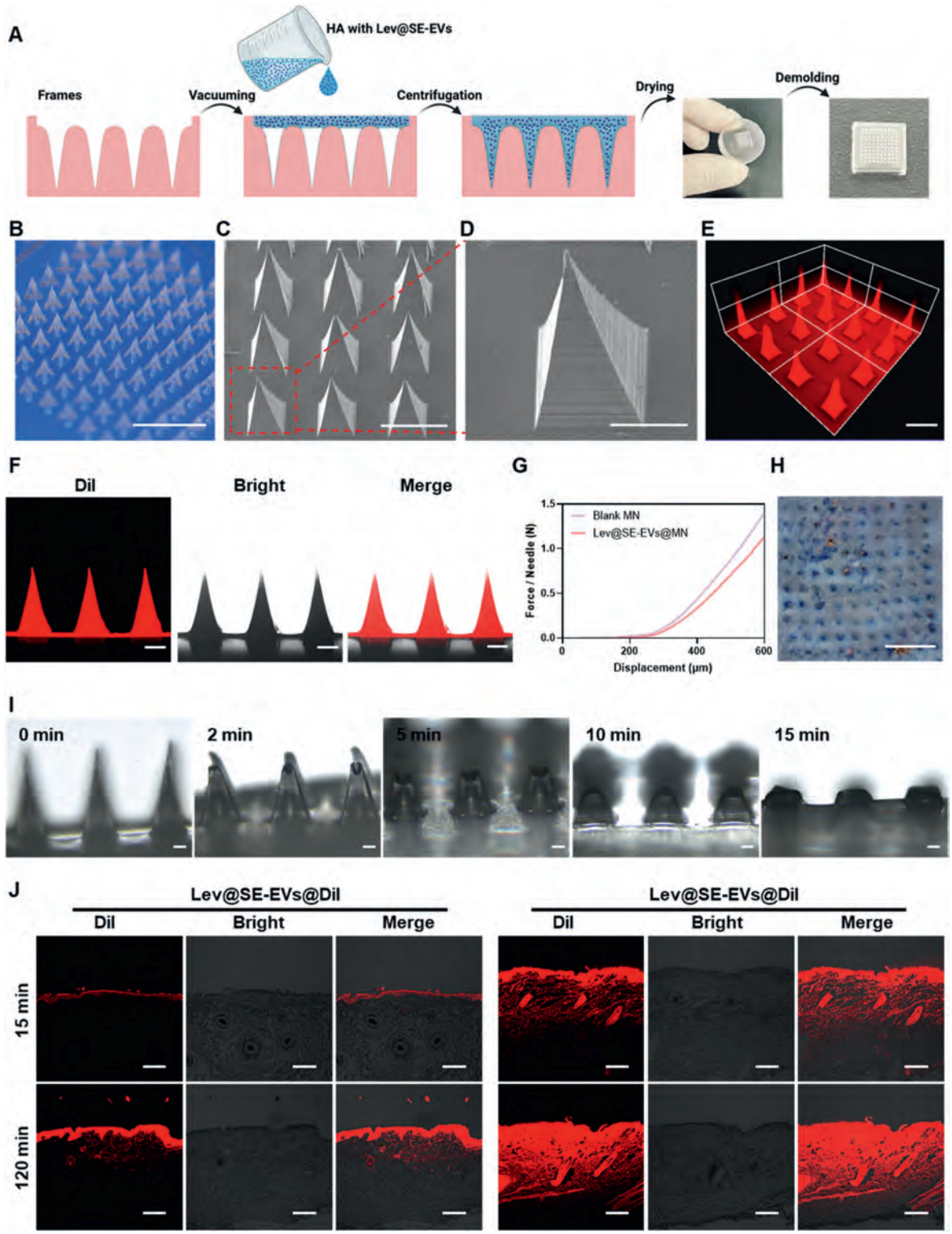

Figure 6 Preparation and characterization of HA-based MN patches containing Lev@SE-EVs (Lev@SE-EVs@MN). (A) Schematic diagram of the Lev@SE-EVs@MN the fabrication procedure using micro-molding method. (B) Optical image of Lev@SE-EVs@MN. Scale bar = 2 mm. (C) Scanning electron microscope image of Lev@SE-EVs@MN. Scale bar = 500 μm. (D) A magnified version of part of the image in panel C. Scale bar = 200 μm. (E) Stereoscopic CLSM image of loading DiI-labeled Lev@SE-EVs into MN (Lev@SE-EVs@DiI@MN). Scale bar = 500 μm. (F) CLSM image of Lev@SE-EVs@DiI@MN. Scale bar = 200 μm. (G) The mechanical strength of Blank MN and Lev@SE-EVs@MN. (H) Stereoscopic micrograph of excised mouse skin after the insertion of loading methylene blue (MB) into HA-based MN patches (MB@MN) *in vitro*. Each blue spot represented the location where each MN top punctured into the skin. Scale bar = 2 mm. (I) Dissolution of Lev@SE-EVs@MN after puncturing mouse skin at the indicated time points. Scale bar = 100 μm. (J) CLSM images after the topical administration of Lev@SE-EVs@DiI and Lev@SE-EVs@DiI@MN on mouse skin. Scale bar = 200 μm.

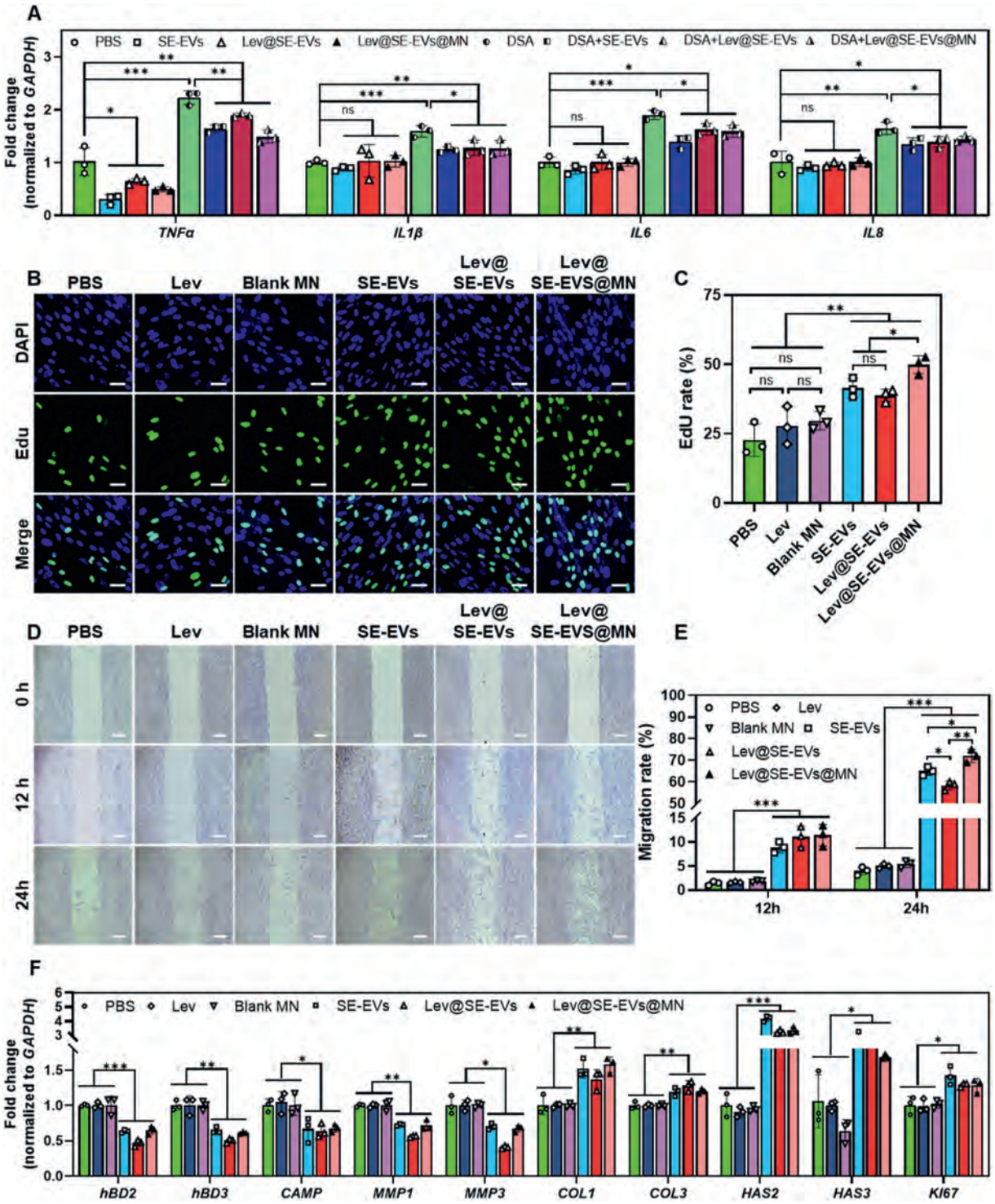

Figure 7 Effect of Lev@SE-EVs@MN on the dermal region. (A) The mRNA levels of *TNFα*, *IL1β*, *IL6*, and *IL8* in HDF cells treated with PBS, SE-EVs, Lev@SE-EVs, Lev@SE-EVs@MN, dead *S. aureus* (DSA), DSA plus SE-EVs, DSA plus Lev@SE-EVs and DSA plus Lev@SE-EVs@MN for 24 h. (B) The proliferation of DSA-treated HDF cells treated with PBS, Lev, Blank MN, SE-EVs, Lev@SE-EVs, and Lev@SE-EVs@MN for 24 h. Scale bar = 50 μm. (C) Quantitative analyses of the proliferation percentage in different groups. (D) The migration of DSA-treated HDF cells treated with PBS, Lev, Blank MN, SE-EVs, Lev@SE-EVs, and Lev@SE-EVs@MN for 12 and 24 h. Scale bar = 200 μm. (E) Quantitative analyses of the migration percentage in different groups. (F) The mRNA levels of *hBD2*, *hBD3*, *CAMP*, *MMP1*, *MMP3*, *COL1*, *COL3*, *HAS2*, *HAS3*, and *KI67* in DSA-treated HDF cells treated with PBS, Lev, Blank MN, SE-EVs, Lev@SE-EVs and Lev@SE-EVs@MN for 24 h. All data are reported as the mean ± SD ($n = 3$). ***$P < 0.001$, **$P < 0.01$, and *$P < 0.05$ as determined by Student's *t* test and one-way ANOVA. ns, no significance.

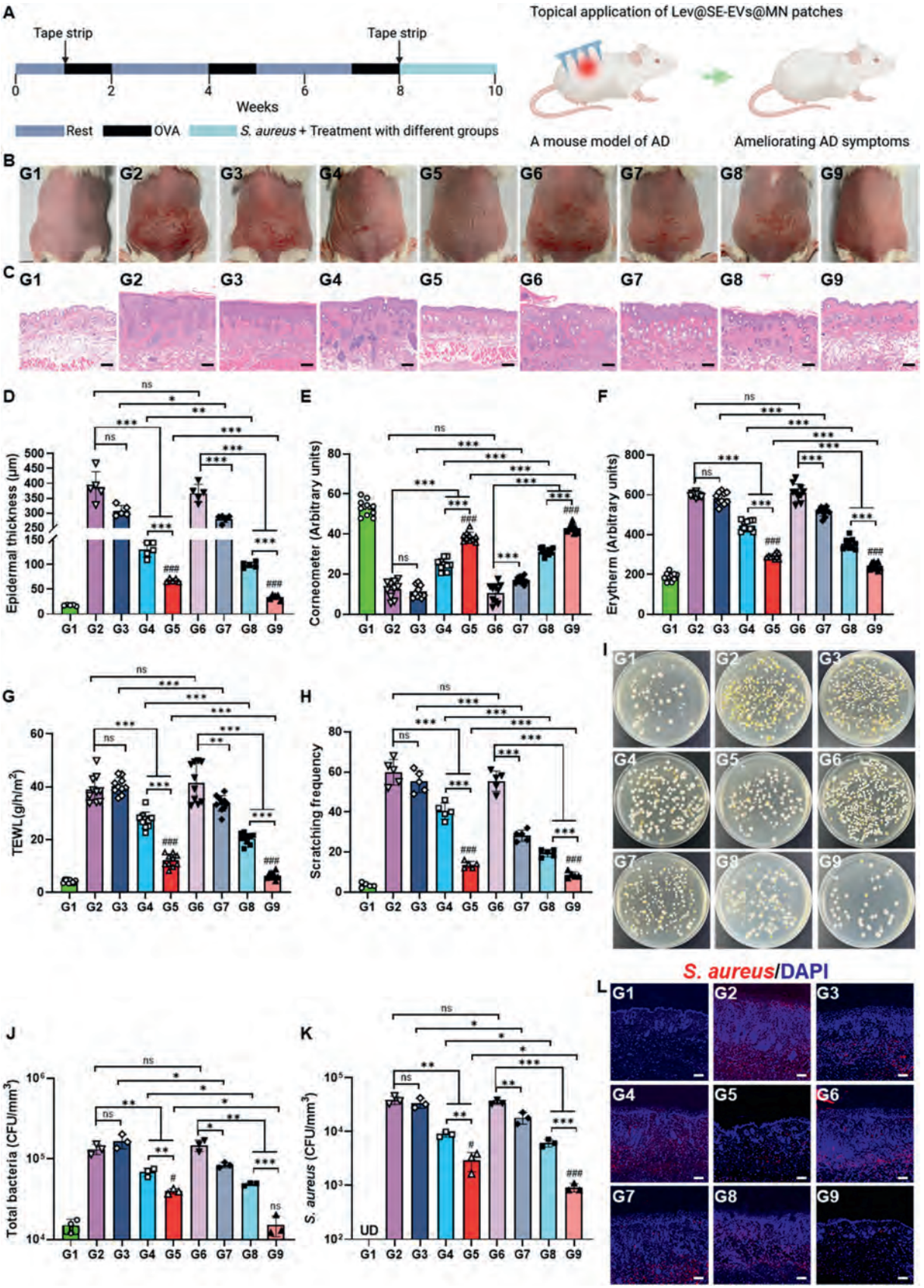

Figure 8 Lev@SE-EVs@MN ameliorated lesion formation in bacterial infection AD mouse model. (A) Schematic illustration of Lev@SE-EVs@MN patch for the treatment of bacterial infection AD. (B) Overall appearance of mouse dorsal skin in different groups at the end of Week 10. (C) H&E staining of mouse dorsal skin from different groups at the end of Week 10. Scale bar = 100 μm. (D) Epidermal thickness of

dependent manner, but only had a slight or negligible benefit on *E. coli* and *P. acnes*, hinting their preferential stimulation on the growth of specific strains in the skin microbiota that could be explained by effective uptake with SE-EVs. Collectively, these data demonstrate that SE-EVs promoted the growth of the *Staphylococcus* genus by selective uptake, and Lev@SE-EVs have a higher cellular uptake efficiency against *S. aureus* than against *S. epidermidis* within the *Staphylococcus* genus, which will specifically target *S. aureus* in AD lesional skin.

3.5. Microneedle (MN)-assisted transdermal delivery of Lev@SE-EVs into the dermis

HA is a natural polysaccharide occurring in corneal skin that can absorb water up to 1000 times in weight, keeping the skin moist to facilitate transdermal delivery. Due to its good solubility and biocompatibility, HA has been widely applied for dissolving MN fabrication to achieve the desired transdermal penetration effect[42]. The Lev@SE-EVs@MN patch composed of HA and Lev@SE-EVs was fabricated through a micro-molding method (Fig. 6A). Considering the antimicrobial effect and biocompatibility, Lev@SE-EVs were added at a dose of 9.92×10^9 particles/mL. The resulting MN displayed a pyramidal needle shape with a needle height of approximately 620 μm (Fig. 6B−D). As seen in the fluorescence images of DiI-labeled Lev@SE-EVs-loaded MN (Lev@SE-EVs@DiI@MN), red fluorescence was homogenously distributed in the MN patch, indicating the Lev@SE-EVs were successfully loaded into the MN and evenly distributed (Fig. 6E and F). The mechanical properties of blank MN (without Lev@SE-EVs) and Lev@SE-EVs@MN were 1.40 N and 1.13 N per needle (Fig. 6G), respectively, which was remarkably higher than the minimum strength of 0.1 N required to puncture the skin[43]. Microscopy images of each membrane of parafilm M® displayed that the Lev@SE-EVs@MN array reaches at least the fifth membrane layer (Supporting Information Fig. S3) and methylene blue staining clearly shows the formation of microchannels in mouse skin after MN treatment, further confirming the effective skin penetration of the Lev@SE-EVs@MN (Fig. 6H). After skin insertion, Lev@SE-EVs@MN dissolved completely in the skin tissue within 15 min (Fig. 6I). A wider distribution of red fluorescence at 15 min and even at 120 min was noted in the skin treated with Lev@SE-EVs@DiI@MN compared to Lev@SE-EVs@DiI (Fig. 6J), indicating the MN facilitated the release and accumulation of the loaded cargo in the dermis. Note that loading Lev@SE-EVs into MN did not affect its inherent properties, such as particle size, zeta potential, protein, and antimicrobial effect (Table S1 and Supporting Information Fig. S4). In summary, these results suggest that Lev@SE-EVs@MN exhibited a sharp needle morphological structure and proper mechanical properties to penetrate the skin, and could transport the loaded cargoes to the dermal region.

3.6. Effect of Lev@SE-EVs@MN on the dermal region

Entry of *S. aureus* into the dermis triggers immune abnormalities and stimulates the production of proinflammatory cytokines[4]. To investigate the effects of Lev@SE-EVs@MN on the dermal region, the interaction between fibroblasts and Lev@SE-EVs@MN was investigated by two independent approaches. Firstly, as shown in Fig. 7A, Lev@SE-EVs@MN did not induce the expression of proinflammatory genes (*TNFα*, *IL1β*, *IL6*, and *IL8*) in HDF cells, whereas Lev@SE-EVs@MN significantly decreased these genes in dead *S. aureus* (DSA)-treated HDF cells. Next, whether Lev@SE-EVs@MN could promote dermal cell renewal was explored. As shown in Fig. 7B−E, Lev@SE-EVs@MN significantly increased the proliferation and migration of DSA-treated HDF cells. In addition, Lev@SE-EVs@MN remarkably decreased the expression of *MMP1* and *MMP3* and increased the expression of *COL1*, *COL3*, *HAS2*, *HAS3* and *KI67* in DSA-treated HDF cells (Fig. 7F). Notably, the mRNA levels of AMP (*hBD2*, *hBD3* and *CAMP*) were significantly decreased in DSA-treated HDF cells incubated with Lev@SE-EVs@MN (Fig. 7F). Similar results were observed in SE-EVs and Lev@SE-EVs (Fig. 7A−F). Besides, these results were further demonstrated at the protein level for certain genes (MMP1, MMP3, COL1, and COL3, Supporting Information Fig. S5A−S5E). Collectively, these findings indicate that Lev@SE-EVs released by Lev@SE-EVs@MN repaired skin by attenuating inflammation and promoting HDF cell renewal in the dermal region and compensated antimicrobial barrier in the dermis due to the absence of initial immune activation in DSA-treated HDF cells.

Secondly, whether the interaction between fibroblasts and Lev@SE-EVs released by Lev@SE-EVs@MN was confirmed in mice. Compared with PBS-treated L929 cells, Lev@SE-EVs@MN did not induce the expression of proinflammatory genes (*Tnfα*, *Il6*, and *Il8*) in L929 cells, whereas Lev@SE-EVs@MN significantly decreased these genes in DSA-induced L929 cells (Fig. S5F). In addition, Lev@SE-EVs@MN significantly decreased the expression of *Mmp1* and *Mmp3* and increased the expression of *Col1* and *Col3* in DSA-treated L929 cells (Fig. S5G). Similar to DSA-treated HDF cells incubated with Lev@SE-EVs@MN, Lev@SE-EVs@MN did not induce the expression of mouse β-defensin (*mBD*) 4, *mBD3* and *mBD14* in DSA-treated L929 cells (Fig. S5G). Similar results were observed in SE-EVs and Lev@SE-EVs (Fig. S5F and S5G). Considering that the shape of the MN does not match the wound, the *S. aureus* infection model was applied to the mouse skin wound to estimate

H&E-stained tissue sections from different groups at the end of Week 10 ($n = 5$). (E−G) The corneometer, erytherm, and TEWL of mouse dorsal skin from different groups at the end of Week 10 ($n = 10$). (H) The scratching frequency of mice from different groups at the end of Week 10 ($n = 5$). (I−K) The mouse dorsal skin from different groups at the end of Week 10 was collected, homogenized, and diluted at 1:10,000 to spread on plates. After incubation at 37 °C for 36 h, total bacterial colonies and *S. aureus* (visible as yellow-colored colonies) were counted and subsequently calculated ($n = 3$). (L) Immunofluorescence images of the mouse dorsal skin from different groups at the end of Week 10 (blue: DAPI; red: *S. aureus*). Scale bar = 100 μm. G1, normal mice; G2, a mouse model where AD was induced by repeated epicutaneous sensitization of tape-stripped skin with OVA, followed by infection with *S. aureus*; G3, a mouse model treated with Lev; G4, a mouse model treated with SE-EVs; G5, a mouse model treated with Lev@SE-EVs; G6, a mouse model treated with blank MN; G7, a mouse model treated with Lev@MN; G8, a mouse model treated with SE-EVs@MN; G9, a mouse model treated with Lev@SE-EVs@MN. Data are reported as the mean ± SD. $^{***}P < 0.001$, $^{**}P < 0.01$ and $^{*}P < 0.05$ as determined by Student's *t* test. $^{\#\#\#}P < 0.001$, $^{\#\#}P < 0.01$, and $^{\#}P < 0.05$ as determined by Student's *t* test and one-way ANOVA, compared with the G1. ns, no significance. UD, undetectable.

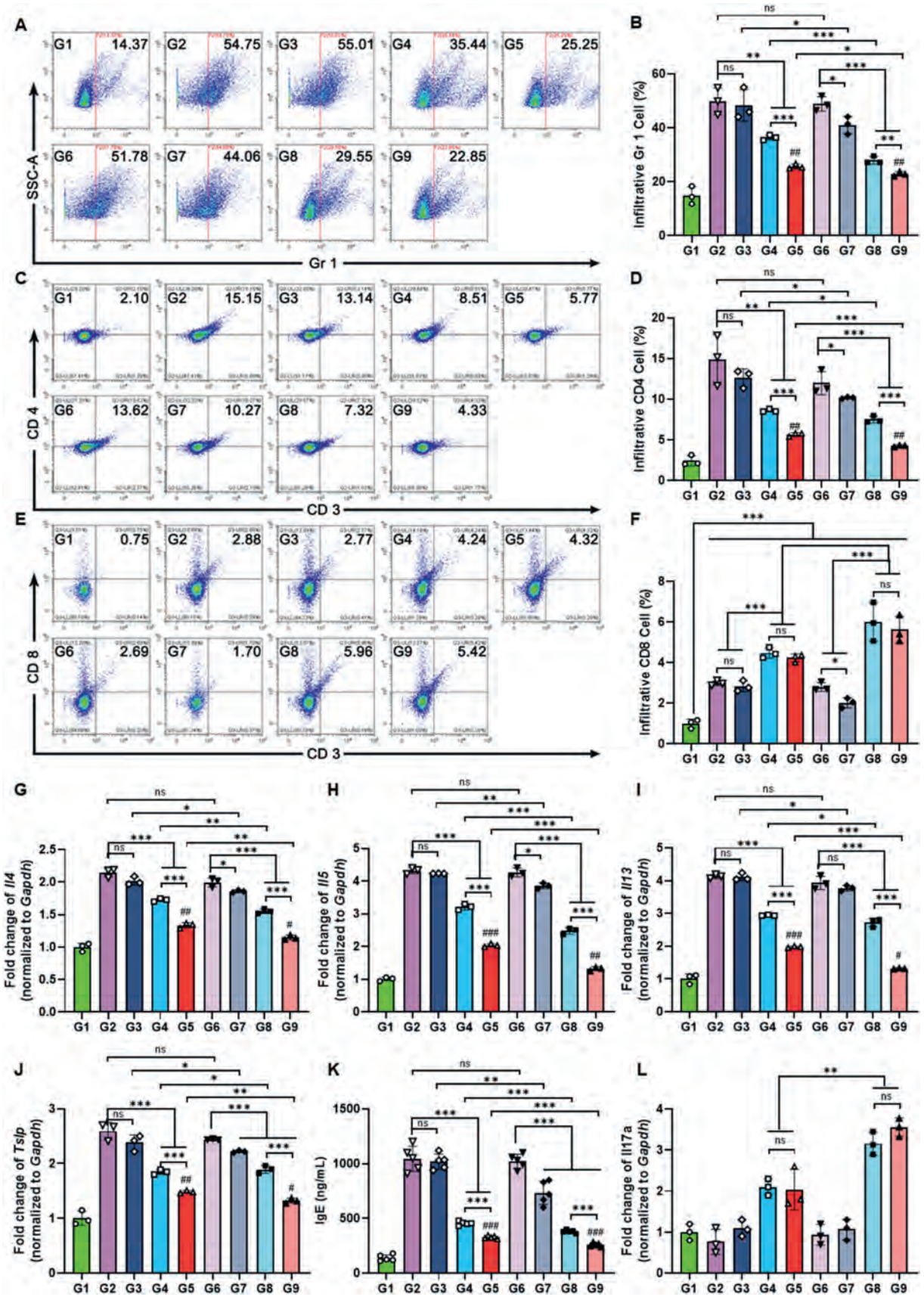

Figure 9 Lev@SE-EVs ameliorated inflammatory cell infiltration in bacterial infection AD mouse model. (A–F) Flow cytometry analysis and corresponding quantitative analyses of $Gr1^+$ cells (A, B), $CD4^+$ T cells (C, D), and $CD8^+$ T cells (E, F) of mouse dorsal skin in different

the *in vivo* repaired efficiency using Lev@SE-EVs. As shown in Fig. S5H−S5J, the shrinking size and reduced bacterial amount in the infected wound of mice treated with Lev@SE-EVs was far more significant compared with that of other treatments. In addition, a minimum number of inflammatory cell infiltration and fibroblast proliferation were observed in the infected wounds of mice treated with Lev@SE-EVs (Fig. S5K).

3.7. Treatment of bacterial infection atopic dermatitis by Lev@SE-EVs@MN patch

Patients with defects in the skin barrier such as AD are more prone to colonization and infection by *S. aureus*, a factor that exacerbates disease[4,44]. To evaluate the therapeutic potential of the MN patch against bacterial infection AD, the mouse model of AD was established by applying *S. aureus* on the tape-stripped dorsal skin induced by repeated epicutaneous sensitization with ovalbumin (Fig. 8A). Lev@MN, SE-EVs, Lev@SE-EVs, SE-EVs@MN and Lev@SE-EVs@MN markedly mitigated typical lesion (such as scaling, dryness, redness, TEWL, and scratching behaviors; Fig. 8B, E−H), histopathologic features of AD-like dermatitis (such as hyperkeratosis, epidermal hyperplasia, and inflammatory cell infiltration; Fig. 8C and D), and overall bacterial burden as well as infection of *S. aureus* (Fig. 8I−L), in the mouse model of AD. The efficacy against AD was in the order of Lev@SE-EVs@MN > SE-EVs@MN > Lev@SE-EVs > SE-EVs > Lev@MN. However, Lev and blank MN showed no therapeutic effect. In sharp contrast, regardless of Lev, SE-EVs, or Lev@SE-EVs, the treatment *via* MN administration generated a better therapeutic effect. In addition, compared with the control (mice treated with PBS), no substantial body weight loss and hemolysis were observed in the mice treated with other treatments during the treatment period (Supporting Information Fig. S6A and S6B), suggesting safe characteristics of Lev@SE-EVs@MN. Together, these data demonstrate that MN contributed to transdermal delivery and Lev@SE-EVs@MN could enhance barrier repair and decrease bacterial infection in bacterial infection AD.

The effects of Lev@SE-EVs@MN on inflammatory cell infiltration in an OVA-sensitized and tape-stripped AD-like dermatitis mouse model with *S. aureus* infection was subsequently investigated. Topical application of SE-EVs, Lev@SE-EVs, Lev@MN, SE-EVs@MN, and Lev@SE-EVs@MN substantially reduced the abundances of $Gr1^+$ cells and $CD4^+$ T cells (Fig. 9A−D), Th2 cytokine gene expression (*Il4*, *Il5*, *Il13*, and *Tslp*; Fig. 9G−J) and total serum IgE levels (Fig. 9K) compared with an untreated mouse model, whereas topical application of Lev and blank MN did not. Among various treatments, topical application of Lev@SE-EVs@MN exhibited the strongest inhibition of inflammatory cell infiltration. Notably, a significant increase in $CD8^+$ T cells with the transcription of *Il17a* was observed in the mouse model of AD after treatment with SE-EVs, Lev@SE-EVs, SE-EVs@MN, and Lev@SE-EVs@MN (Fig. 9E, F, L). There was no difference in the number of IL-$17A^+$ $CD8^+$ T cells between SE-EVs and Lev@SE-EVs or between SE-EVs@MN and Lev@SE-EVs@MN. Regardless of SE-EVs or Lev@SE-EVs, the application *via* MN administration induced a greater number of IL-$17A^+$ $CD8^+$ T cells. These findings suggest that Lev@SE-EVs@MN mitigated inflammatory cell infiltration, expression of Th2 cytokine genes, and IgE levels in the mouse model of AD.

4. Discussion

In this study, we demonstrated that Lev@SE-EVs regulated epidermal immune responses and enhanced epidermal barrier in normal mice. Upon insertion into the skin, the rapidly released Lev@SE-EVs from the MN selectively killed *S. aureus*, decreased inflammatory cell infiltration, and enhanced skin repairing in the bacterial infection AD mouse model. Lev@SE-EVs induced accumulation of IL-$17A^+$ $CD8^+$ T cells in the skin in an unrelated inflammatory manner. Our results pointed toward the role of MN-assisted Lev@SE-EVs in improving bacterial infection, skin inflammation, and skin repair.

The repeated freeze-anneal-thaw method is a widely applied technique to increase the encapsulation efficiency of liposomes[40]. Since EVs are structurally similar to liposomes, we encapsulated Lev into SE-EVs to obtain Lev@SE-EVs by this method. There were some differences in physical properties (including the particle size and PDI) before and after loading. The lipid bilayer of SE-EVs may fuse after freezing, leading to an increase in particle size and PDI. Costa et al.[40] have observed similar particle size increases after drug loading in EVs. However, owing to their cellular origin[45], there are no significant changes in zeta potential and protein before and after loading. For the functional properties, except the antimicrobial capacity, the functions of Lev@SE-EVs are largely similar to that of SE-EVs, such as anti-inflammatory, modulating epidermal immunity, and enhancing epidermal barrier, suggesting that loading Lev into SE-EVs has a negligible effect on its functionality. However, since EVs are complex, the impact of this method on the function of SE-EVs may need detailed investigation. Compared to free Lev, Lev@SE-EVs has stronger antibacterial activity against *S. aureus*, avoiding the risk of bacterial resistance. In addition, the particle concentration of Lev@SE-EVs was measured by NTA, which will contribute to the development of personalized precision therapies by tailoring the dose to individual needs.

Patients with AD have an impaired skin (epidermal and dermal) barrier including physicochemical and antimicrobial barriers, which are often associated with colonization and infection by *S. aureus*[4,38,46]. Although *S. aureus* can penetrate the epidermis by a proteolytic mechanism in healthy skin, an impaired epidermal barrier results in increased susceptibility to the skin pathogen *S. aureus*[46]. In addition, the decreased antimicrobial barrier (CAMP, hBD2, and hBD3) of AD patient skin enhances

treatments at the end of Week 10 ($n = 3$). (G−J) The mRNA levels of different *Th2* cytokine genes (*Il4*, *Il5*, *Il13*, and *Tslp*) in the mouse dorsal skin in different groups at the end of Week 10 ($n = 3$). (K) The total serum IgE levels of mice in different groups at the end of Week 10 ($n = 5$). (L) The IL-17A mRNA levels in the mouse dorsal skin in different groups at the end of Week 10 ($n = 3$). G1, normal mice; G2, a mouse model where AD was induced by repeated epicutaneous sensitization of tape-stripped skin with OVA, followed by infection with *S. aureus*; G3, a mouse model treated with Lev; G4, a mouse model treated with SE-EVs; G5, a mouse model treated with Lev@SE-EVs; G6, a mouse model treated with blank MN; G7, a mouse model treated with Lev@MN; G8, a mouse model treated with SE-EVs@MN; G9, a mouse model treated with Lev@SE-EVs@MN. Data are reported as the mean ± SD. $^{***}P < 0.001$, $^{**}P < 0.01$, and $^{*}P < 0.05$ as determined by Student's *t* test and one-way ANOVA. $^{\#\#\#}P < 0.001$, $^{\#\#}P < 0.01$, and $^{\#}P < 0.05$ as determined by Student's *t* test, compared with the G1. ns, no significance.

the entry of *S. aureus* into the dermis. The entry of *S. aureus* allows them to direct contact with viable immune cells, trigger the secretion of pro-inflammatory cytokines, and destroy proteolytic homeostasis by inducing multiple metalloproteases[4], which results in a positive correlation between the abundance of *S. aureus* in AD and disease severity. In this study, we showed that Lev@SE-EVs enhanced epidermal barrier function by increasing epidermal barrier integrity in normal murine skin and promoting the expression of AMPs in HaCaT cells, suggesting that Lev@SE-EVs enhance epidermal barrier function to reduce susceptibility to *S. aureus*. However, it remains to be determined whether the application of Lev@SE-EVs *via* MN administration has a much better effect on the epidermis and how Lev@SE-EVs restore epidermal barrier function in the AD mouse model. In the dermis, Lev@SE-EVs released from the MN insertion suppressed inflammation while promoting repair in DSA-treated HDF cells. Similar results were observed in mice *in vivo* and *in vitro*. These results indicate the potential of Lev@SE-EVs for inhibiting inflammation and repairing the damage to the dermis layer in AD. Notably, both SE-EVs and Lev@SE-EVs did not induce *hBD2*, *hBD3*, and *CAMP* in DSA-HDF cells. Although similar to SE-EVs in function, Lev@SE-EVs compensate for the deficiency of antimicrobial barrier in the dermis.

Considering that *S. aureus* is more abundant in the dermis of AD lesional skin[4] and that nanocarrier penetration into the dermis is pretty limited[47], we loaded Lev@SE-EVs into HA-based MN (Lev@SE-EVs@MN) to enhance the skin penetration. MN enables efficient transdermal delivery of Lev@SE-EVs into inflamed epidermis and dermis, where Lev@SE-EVs are further taken up by the targeted cells to perform their respective functions. Regardless of Lev, SE-EVs, or Lev@SE-EVs, the application *via* MN administration showed a better therapeutic effect compared with the application without MN. As expected, Lev@SE-EVs@MN significantly reduced the number of *S. aureus* in the dermis compared with SE-EVs@MN. Notably, the application of blank HA-based MN did not significantly reduce inflammation in the infected AD mouse model, indicating that HA may be only suitable for mild AD.

Recent studies on skin microbiota-derived EVs mainly focus on skin microbiota−host interactions (being beneficial or harmful to skin homeostasis)[25,48,49]. However, the role of commensal EVs in skin microecology goes far beyond this, especially in the selective regulation of microbiota composition. In this study, we presented that SE-EVs increased the abundance of beneficial commensal taxa belonging to the phylum *Firmicutes* (*i.e.*, *Staphylococcus* spp.) in normal mice. Previous studies have shown that EVs are more likely to be uptaken by cells with similar membrane structures[36]. SE-EVs-mediated modulation of the skin microbiota was accomplished through preferential uptake by the *Staphylococcus* genus, which was supported by the fact that SE-EVs robustly promoted the growth of the *Staphylococcus* genus among the skin microbiota. In addition, the cellular uptake of SE-EVs was higher in *S. aureus* than in *S. epidermidis* despite both belonging to the *Staphylococcus* genus, which might be associated with inconsistent growth rates of bacteria or inherent characteristics of SE-EVs. The underlying mechanisms of preferential uptake between bacteria and SE-EVs warrant further investigation. Notably, loading Lev into SE-EVs did not affect bacterial cellular uptake of Lev@SE-EVs, and Lev@SE-EVs were more taken up by *S. aureus*, which will be much less likely to harm the indigenous microbiota in AD lesional skin due to selective killing of *S. aureus*.

There is a strong correlation between the specific $CD8^+$ T-cell level and the disease severity in AD[50,51]. In this study, we revealed that the application of Lev@SE-EVs or SE-EVs with/without MN significantly reduced inflammatory cell infiltration ($Gr1^+$ cells and $CD4^+$ T cells) but increased $CD8^+$ T cells in bacterial infection AD. Different from IFN-γ^+ $CD8^+$ T cells in lesional AD skin, the increased $CD8^+$ T cells have a distinct cytokine profile characterized by the production of IL-17A, which is consistent with our previous report[25]. In addition, Lev@SE-EVs or SE-EVs could induce IL-$17A^+$ $CD8^+$ T cells in normal mice. These results indicate that IL-$17A^+$ $CD8^+$ T-cell response is not related to inflammation. Prior studies have shown that colonization with *S. epidermidis* induces IL-$17A^+$ $CD8^+$ T cells to accumulate in the skin in an unrelated-inflammation manner, thus enhancing the innate immunity barrier and limiting pathogen invasion[15]. Therefore, the commensal-specific T-cell response could be induced by SE-EVs. Interestingly, topical application of Lev@SE-EVs or SE-EVs decreased inflammatory cell infiltration ($Gr1^+$ cells and $CD4^+$ T cells) in normal mice, suggesting the potential of SE-EVs-based nanocarriers in anti-inflammatory and anti-sensitive cosmetics. In addition, Lev@SE-EVs or SE-EVs *via* MN administration induced more IL-$17A^+$ $CD8^+$ T cells than without MN, implying a synergistic effect of MN.

5. Conclusions

In summary, our findings disclosed the versatility of Lev@SE-EVs in selectively killing *S. aureus*, anti-inflammatory, repairing skin, and improving Th2 lymphocyte skewing. Notably, the application of Lev@SE-EVs *via* MN exhibited the strongest therapy effect for the treatment of bacterial infection AD. It is anticipated that these observations will inspire more innovative ideas focused on drug delivery of SE-EVs-based nanocarriers for skin disease intervention and treatment.

Acknowledgments

This work was partially supported by: National Natural Science Foundation of China (Grant Nos. 31470968 and 32101068), National key R & D program of Nanotechnology of China (Grant Nos. 2020YFA0710700), National Basic Research Program of China (Grant Nos. 2022YFA1206000), Jiangsu Distinguished Professor Program (China). The authors thank the Analytical and Testing Center of the College of Life Science and Technology in Huazhong University of Science and Technology for their help. Sequencing service and data analysis service were provided by Wekemo Tech Group Co., Ltd. Shenzhen China.

Author contributions

Hong Zhou: Writing − review & editing, Writing − original draft, Visualization, Supervision, Methodology, Investigation, Conceptualization. Shuting Zhang: Visualization, Methodology, Investigation. Xinxin Liu: Visualization, Methodology, Investigation. Aiping Feng:Visualization, Methodology, Investigation. Siyuan Chen: Writing − review & editing, Writing − original draft, Visualization, Supervision, Methodology, Investigation, Funding acquisition, Conceptualization. Wei Liu: Writing − review & editing, Writing − original draft, Visualization, Supervision, Methodology, Investigation, Funding acquisition, Conceptualization.

Conflicts of interest

The authors have no conflicts of interest to declare.

Appendix A. Supporting information

Supporting information to this article can be found online at https://doi.org/10.1016/j.apsb.2025.02.038.

References

1. Eckert L, Gupta S, Amand C, Gadkari A, Mahajan P, Gelfand JM. The burden of atopic dermatitis in us adults: health care resource utilization data from the 2013 national health and wellness survey. *J Am Acad Dermatol* 2018;**78**:54−61.
2. Wu H, Ke X, Huang W, Shi W, Yao S, Duan YY, et al. Multitissue integrative analysis identifies susceptibility genes for atopic dermatitis. *J Invest Dermatol* 2023;**143**:602−11.
3. Lio PA, Lee M, LeBovidge J, Timmons KG, Schneider L. Clinical management of atopic dermatitis: practical highlights and updates from the atopic dermatitis practice parameter 2012. *J Aller Cl Immpract* 2014;**2**:361−9.
4. Nakatsuji T, Chen TH, Two AM, Chun KA, Narala S, Geha RS, et al. *Staphylococcus aureus* exploits epidermal barrier defects in atopic dermatitis to trigger cytokine expression. *J Invest Dermatol* 2016;**136**: 2192−200.
5. Suh L, Coffin S, Leckerman KH, Gelfand JM, Honig PJ, Yan AC. Methicillin-resistant *Staphylococcus aureus* colonization in children with atopic dermaitis. *Pediatr Dermatol* 2008;**25**:528−34.
6. Kusumi Y, Ando Y, Shigeyasu C, Fukui M, Yamada M. Levofloxacin susceptibility of staphylococci from conjunctiva in patients with atopic dermatitis. *Jpn J Ophthalmol* 2024;**68**:134−8.
7. Niebuhr M, Mai U, Kapp A, Werfel T. Antibiotic treatment of cutaneous infections with *Staphylococcus aureus* in patients with atopic dermatitis: current antimicrobial resistances and susceptibilities. *Exp Dermatol* 2008;**17**:953−7.
8. Kim J, Kim BE, Ahn K, Leung DYM. Interactions between atopic dermatitis and *Staphylococcus aureus* infection: clinical implications. *Allergy Asthma Immun* 2019;**11**:593−603.
9. Byrd AL, Deming C, Cassidy SKB, Harrison OJ, Ng WI, Conlan S, et al. *Staphylococcus aureus* and *Staphylococcus epidermidis* strain diversity underlying pediatric atopic dermatitis. *Sci Transl Med* 2017; **9**:eaal4651.
10. Huang JT, Abrams M, Tlougan B, Rademaker A, Paller AS. Treatment of *Staphylococcus aureus* colonization in atopic dermatitis decreases disease severity. *Pediatrics* 2009;**123**:e808−14.
11. Ring J, Alomar A, Bieber T, Deleuran M, Fink-Wagner A, Gelmetti C, et al. Guidelines for treatment of atopic eczema (atopic dermatitis) part i. *J Eur Acad Dermatol Venereol* 2012;**26**:1045−60.
12. Eriksson S, van der Plas MJA, Mörgelin M, Sonesson A. Antibacterial and antibiofilm effects of sodium hypochlorite against *Staphylococcus aureus* isolates derived from patients with atopic dermatitis. *Br J Dermatol* 2017;**177**:513−21.
13. George SMC, Karanovic S, Harrison DA, Rani A, Birnie AJ, Bath-Hextall FJ, et al. Interventions to reduce *Staphylococcus aureus* in the management of eczema: updated cochrane systematic review. *Br J Dermatol* 2020;**183**:146.
14. Yarbrough KB, Neuhaus KJ, Simpson EL. The effects of treatment on itch in atopic dermatitis. *Dermatol Ther* 2013;**26**:110−9.
15. Naik S, Bouladoux N, Linehan JL, Han SJ, Harrison OJ, Wilhelm C, et al. Commensal-dendritic-cell interaction specifies a unique protective skin immune signature. *Nature* 2015;**520**:104−8.
16. Lai Y, Cogen AL, Radek KA, Park HJ, Macleod DT, Leichtle A, et al. Activation of tlr2 by a small molecule produced by *Staphylococcus epidermidis* increases antimicrobial defense against bacterial skin infections. *J Invest Dermatol* 2010;**130**:2211−21.
17. Cogen AL, Yamasaki K, Sanchez KM, Dorschner RA, Lai Y, MacLeod DT, et al. Selective antimicrobial action is provided by phenol-soluble modulins derived from *Staphylococcus epidermidis*, a normal resident of the skin. *J Invest Dermatol* 2010;**130**:192−200.
18. Lai Y, Di Nardo A, Nakatsuji T, Leichtle A, Yang Y, Cogen AL, et al. Commensal bacteria regulate toll-like receptor 3-dependent inflammation after skin injury. *Nat Med* 2009;**15**:1377−82.
19. Nakatsuji T, Chen TH, Narala S, Chun KA, Two AM, Yun T, et al. Antimicrobials from human skin commensal bacteria protect against *Staphylococcus aureus* and are deficient in atopic dermatitis. *Sci Transl Med* 2017;**9**:eaah4680.
20. Zhou H, Shi LL, Ren YY, Tan X, Liu W, Liu Z. Applications of human skin microbiota in the cutaneous disorders for ecology-based therapy. *Front Cell Infect Microbiol* 2020;**10**:570261.
21. Stacy A, Belkaid Y. Microbial guardians of skin health. *Science* 2019; **363**:227−8.
22. Zheng Y, Hunt RL, Villaruz AE, Fisher EL, Liu R, Liu Q, et al. Commensal *Staphylococcus epidermidis* contributes to skin barrier homeostasis ceramides. *Cell Host Microbe* 2022;**30**:301−13.
23. Shao S, Fang H, Li QY, Wang G. Extracellular vesicles in inflammatory skin disorders: from pathophysiology to treatment. *Theranostics* 2020;**10**:9937−55.
24. McBride JD, Rodriguez-Menocal L, Badiavas EV. Extracellular vesicles as biomarkers and therapeutics in dermatology: a focus on exosomes. *J Invest Dermatol* 2017;**137**:1622−9.
25. Zhou H, Tan X, Chen G, Liu X, Feng A, Liu Z, et al. Extracellular vesicles of commensal skin microbiota alleviate cutaneous inflammation in atopic dermatitis mouse model by reestablishing skin homeostasis. *J Invest Dermatol* 2025;**145**:312−22.e9.
26. Gómez-Chávez F, Cedillo-Peláez C, Zapi-Colín LA, Gutiérrez-González G, Martínez-Torres I, Peralta H, et al. The extracellular vesicles from the commensal *Staphylococcus epidermidis* atcc12228 strain regulate skin inflammation in the imiquimod-induced psoriasis murine model. *Int J Mol Sci* 2021;**22**:13029.
27. Wang XY, Lin SS, Wang L, Cao ZP, Zhang MM, Zhang YF, et al. Versatility of bacterial outer membrane vesicles in regulating intestinal homeostasis. *Sci Adv* 2023;**9**:eade5079.
28. Byrd AL, Deming C, Cassidy SKB, Harrison OJ, Ng WI, Conlan S, et al. *Staphylococcus aureus* and *Staphylococcus epidermidis* strain diversity underlying pediatric atopic dermatitis. *Sci Transl Med* 2017; **9**:eaal4651.
29. Sun Y, Liu JL, Wang HY, Li SS, Pan XT, Xu BL, et al. Nir laser-triggered microneedle-based liquid band-aid for wound care. *Adv Funct Mater* 2021;**31**:2100218.
30. Jing Q, Ruan H, Li J, Wang Z, Pei L, Hu H, et al. Keratinocyte membrane-mediated nanodelivery system with dissolving microneedles for targeted therapy of skin diseases. *Biomaterials* 2021;**278**: 121142.
31. Wan T, Pan Q, Ping Y. Microneedle-assisted genome editing: a transdermal strategy of targeting nlrp3 by crispr-cas9 for synergistic therapy of inflammatory skin disorders. *Sci Adv* 2021;**7**:eabe2888.
32. Gariboldi S, Palazzo M, Zanobbio L, Selleri S, Sommariva M, Balsari A, et al. Low molecular weight hyaluronic acid increases the self defence of skin epithelium by induction of β-defensin 2 *via* tlr2 and 4. *Cytokine* 2008;**181**:2103−10.
33. Zheng BW, Wang B, Xiao WL, Sun YJ, Yang C, Zhao BT. Different molecular weight hyaluronic acid alleviates inflammation response in dnfb-induced mice atopic dermatitis and LPS-induced RAW264.7 cells. *Life Sci* 2022;**301**:120591.
34. Gan J, Zhang X, Ma W, Zhao Y, Sun L. Antibacterial, adhesive, and MSC exosomes encapsulated microneedles with spatio-temporal variation functions for diabetic wound healing. *Nano Today* 2022; **47**:101630.
35. Yerneni SS, Yalcintas EP, Smith JD, Averick S, Campbell PG, Ozdoganlar OB. Skin-targeted delivery of extracellular vesicle-encapsulated curcumin using dissolvable microneedle arrays. *Acta Biomater* 2022;**149**:198−212.

36. Huang W, Zhang Q, Li W, Yuan M, Zhou J, Hua L, et al. Development of novel nanoantibiotics using an outer membrane vesicle-based drug efflux mechanism. *J Control Release* 2020;**317**:1−22.
37. Li ZM, Xia JJ, Jiang LYQ, Tan YM, An YT, Zhu XY, et al. Characterization of the human skin resistome and identification of two microbiota cutotypes. *Microbiome* 2021;**9**:47.
38. Uberoi A, Bartow-McKenney C, Zheng Q, Flowers L, Campbell A, Knight SAB, et al. Commensal microbiota regulates skin barrier function and repair *via* signaling through the aryl hydrocarbon receptor. *Cell Host Microbe* 2021;**29**:1235-48.e8.
39. Naik S, Bouladoux N, Wilhelm C, Molloy MJ, Salcedo R, Kastenmuller W, et al. Compartmentalized control of skin immunity by resident commensals. *Science* 2012;**337**:1115−9.
40. Costa AP, Xu X, Burgess DJ. Freeze-anneal-thaw cycling of unilamellar liposomes: effect on encapsulation efficiency. *Pharm Res* 2014;**31**:97−103.
41. Fluhr JW, Feingold KR, Elias PM. Transepidermal water loss reflects permeability barrier status: validation in human and rodent *in vivo* and *ex vivo* models. *Exp Dermatol* 2006;**15**:483−92.
42. Xiang YM, Lu JL, Mao CY, Zhu YZ, Wang CF, Wu J, et al. Ultrasound-triggered interfacial engineering-based microneedle for bacterial infection acne treatment. *Sci Adv* 2023;**9**:eadf0854.
43. Chen Q, Xiao Z, Wang C, Chen G, Zhang Y, Zhang X, et al. Microneedle patches loaded with nanovesicles for glucose transporter-mediated insulin delivery. *ACS Nano* 2022;**16**:18223−31.
44. Alexander H, Paller AS, Traidl-Hoffmann C, Beck LA, De Benedetto A, Dhar S, et al. The role of bacterial skin infections in atopic dermatitis: expert statement and review from the international eczema council skin infection group. *Br J Dermatol* 2020;**182**:1331−42.
45. Schulz E, Goes A, Garcia R, Panter F, Koch M, Müller R, et al. Biocompatible bacteria-derived vesicles show inherent antimicrobial activity. *J Control Release* 2018;**290**:46−55.
46. Williams MR, Costa SK, Zaramela LS, Khalil S, Todd DA, Winter HL, et al. Quorum sensing between bacterial species on the skin protects against epidermal injury in atopic dermatitis. *Sci Transl Med* 2019;**11**:eaat8329.
47. Tiwari N, Osorio-Blanco ER, Sonzogni A, Esporrín-Ubieto D, Wang H, Calderón M. Nanocarriers for skin applications: where do we stand?. *Angew Chem Int Ed Engl* 2022;**61**:e202107960.
48. Gómez-Chávez F, Cedillo-Peláez C, Zapi-Colín LA, Gutiérrez-González G, Martínez-Torres I, Peralta H, et al. The extracellular vesicles from the commensal *Staphylococcus epidermidis* atcc12228 strain regulate skin inflammation in the imiquimod-induced psoriasis murine model. *Int J Mol Sci* 2021;**22**:13029.
49. Jun SH, Lee JH, Kim SI, Choi CW, Park TI, Jung HR, et al. *Staphylococcus aureus*-derived membrane vesicles exacerbate skin inflammation in atopic dermatitis. *Clin Exp Allergy* 2017;**47**:85−96.
50. Hennino A, Jean-Decoster C, Giordano-Labadie F, Debeer S, Vanbervliet B, Rozières A, et al. $CD8^+$ T cells are recruited early to allergen exposure sites in atopy patch test reactions in human atopic dermatitis. *J Allergy Clin Immunol* 2011;**127**:1064−7.
51. Hennino A, Vocanson M, Toussaint Y, Rodet K, Benetière J, Schmitt AM, et al. Skin-infiltrating $CD8^+$ T cells initiate atopic dermatitis lesions. *J Immunol* 2007;**178**:5571−7.